National Library of Canada
Acquisitions and Bibliographic Services Branch
395 Wellington Street
Ottawa, Ontario
K1A 0N4

Bibliothèque nationale du Canada
Direction des acquisitions et des services bibliographiques
395, rue Wellington
Ottawa (Ontario)
K1A 0N4

*Your file Votre référence*

*Our file Notre référence*

**NOTICE**

**The quality of this microform is heavily dependent upon the quality of the original thesis submitted for microfilming. Every effort has been made to ensure the highest quality of reproduction possible.**

**If pages are missing, contact the university which granted the degree.**

**Some pages may have indistinct print especially if the original pages were typed with a poor typewriter ribbon or if the university sent us an inferior photocopy.**

**Reproduction in full or in part of this microform is governed by the Canadian Copyright Act, R.S.C. 1970, c. C-30, and subsequent amendments.**

**AVIS**

**La qualité de cette microforme dépend grandement de la qualité de la thèse soumise au microfilmage. Nous avons tout fait pour assurer une qualité supérieure de reproduction.**

**S'il manque des pages, veuillez communiquer avec l'université qui a conféré le grade.**

**La qualité d'impression de certaines pages peut laisser à désirer, surtout si les pages originales ont été dactylographiées à l'aide d'un ruban usé ou si l'université nous a fait parvenir une photocopie de qualité inférieure.**

**La reproduction, même partielle, de cette microforme est soumise à la Loi canadienne sur le droit d'auteur, SRC 1970, c. C-30, et ses amendements subséquents.**

Canada

UNIVERSITY OF ALBERTA

# NONLINEAR EVOLUTION OF STIMULATED BRILLOUIN SCATTERING IN AN INHOMOGENEOUS PLASMA

BY

RALF M. OPPITZ ©

A THESIS

SUBMITTED TO THE FACULTY OF GRADUATE STUDIES AND RESEARCH

IN PARTIAL FULFILMENT OF THE REQUIREMENTS FOR THE DEGREE

OF

MASTER OF SCIENCE

IN

THEORETICAL PHYSICS

DEPARTMENT OF PHYSICS

EDMONTON, ALBERTA

SPRING 1995

National Library
of Canada

Acquisitions and
Bibliographic Services Branch

395 Wellington Street
Ottawa, Ontario
K1A 0N4

Bibliothèque nationale
du Canada

Direction des acquisitions et
des services bibliographiques

395, rue Wellington
Ottawa (Ontario)
K1A 0N4

*Your file Votre référence*

*Our file Notre référence*

THE AUTHOR HAS GRANTED AN IRREVOCABLE NON-EXCLUSIVE LICENCE ALLOWING THE NATIONAL LIBRARY OF CANADA TO REPRODUCE, LOAN, DISTRIBUTE OR SELL COPIES OF HIS/HER THESIS BY ANY MEANS AND IN ANY FORM OR FORMAT, MAKING THIS THESIS AVAILABLE TO INTERESTED PERSONS.

L'AUTEUR A ACCORDE UNE LICENCE IRREVOCABLE ET NON EXCLUSIVE PERMETTANT A LA BIBLIOTHEQUE NATIONALE DU CANADA DE REPRODUIRE, PRETER, DISTRIBUER OU VENDRE DES COPIES DE SA THESE DE QUELQUE MANIERE ET SOUS QUELQUE FORME QUE CE SOIT POUR METTRE DES EXEMPLAIRES DE CETTE THESE A LA DISPOSITION DES PERSONNE INTERESSEES.

THE AUTHOR RETAINS OWNERSHIP OF THE COPYRIGHT IN HIS/HER THESIS. NEITHER THE THESIS NOR SUBSTANTIAL EXTRACTS FROM IT MAY BE PRINTED OR OTHERWISE REPRODUCED WITHOUT HIS/HER PERMISSION.

L'AUTEUR CONSERVE LA PROPRIETE DU DROIT D'AUTEUR QUI PROTEGE SA THESE. NI LA THESE NI DES EXTRAITS SUBSTANTIELS DE CELLE-CI NE DOIVENT ETRE IMPRIMES OU AUTREMENT REPRODUITS SANS SON AUTORISATION.

ISBN 0-612-01644-7

Canada

**UNIVERSITY OF ALBERTA**

**RELEASE FORM**

| | |
|---|---|
| **Name of Author:** | Ralf M. Oppitz |
| **Title of Thesis:** | Nonlinear Evolution of Stimulated Brillouin Scattering in an Inhomogeneous Plasma |
| **Degree:** | Master of Science |
| **Year This Degree Granted:** | 1995 |

Permission is hereby granted to the UNIVERSITY OF ALBERTA LIBRARY to reproduce single copies of this thesis and to lend or sell such copies for private, scholarly or scientific research purposes only.

The author reserves other publication rights, and neither the thesis nor extensive extracts from it may be printed or otherwise reproduced without the author's written permission.

Ralf M. Oppitz

Ralf M. Oppitz
Department of Physics
University of Alberta
Edmonton, Alberta
T6G 2J1

April 21, 1995

UNIVERSITY OF ALBERTA

FACULTY OF GRADUATE STUDIES AND RESEARCH

The undersigned certify that they have read, and recommended to the Faculty of Graduate Studies and Research for acceptance, a thesis entitled "Nonlinear Evolution of Stimulated Brillouin Scattering in an Inhomogeneous Plasma" submitted by Ralf M. Oppitz in partial fulfilment of the requirements for the degree of Master of Science in Theoretical Physics.

Prof. W. Rozmus, Supervisor

Prof. Z. Gortel

Prof. J. Samson

Assoc. Prof. S. Shen

Date: April 13, 1995

April 20, 1995

*Dedicated to*

*my Family*

# ABSTRACT

The influence of nonlinear sound waves and an inhomogeneous plasma flow velocity on stimulated Brillouin scattering (SBS) in the regime of weak damping is studied. A local approximation which is based on a driven Korteweg-de Vries (KdV) equation, is used to analyse ion acoustic waves produced by a periodic driving term. When the nonlinear frequency shift of an ion acoustic wave is balanced by the inhomogeneous effects one expects the autoresonance effect to occur. We have studied this process using the KdV model and found that autoresonance is irrelevant for SBS evolution.

The complete study of the SBS evolution in inhomogeneous plasmas has been presented. The SBS reflectivity undergoes convective saturation, and when the damping rate allows it, the instability shows a subsequent stage of absolute growth. At saturation SBS produces an oscillatory reflectivity leading to a decrease in the average reflectivity for an increasing flow inhomogeneity. The flow inhomogeneity causes a broadening of the frequency spectrum of the reflected light. The competition between nonlinearity and inhomogeneity of the flow velocity has been analysed for the first time.

# ACKNOWLEDGEMENTS

I first want to thank my supervisor, Prof. Rozmus, for his support and enthusiasm during the past two and a half years. I also wish to thank professor Valdimir Tikhonchuck for the shreds of physical insight that I have learnt from him. I still have not truly appreciated the countless hours saved by Dr. Andrea Maximov in guiding me through the many mathematical and technical hurdles. I also wish to thank my supervisory committee for the suggestions and feedback they offered.

The support of my parents and grandmother during my studies here was greatly appreciated. The hospitality from my aunt and uncle was gratefully received and provided a welcomed distraction. The encouragement and good will from Ascension Lutheran Church was also gratefully accepted.

I also want to thank all of the people who made my stay in Edmonton pleasant. Jason, Shawn, Joe, Konstintine, Brendon, Bernard, Ivan, Rob, Suresh, Alex, Kevin, Dave, Lynn, and others too numerous to mention deserve special recognition.

# TABLE OF CONTENTS


1 INTRODUCTION TO LASER PLASMA PHYSICS 1

1.1 Introduction . . . . . 1

1.2 Parametric Instabilities . . . . . 3

1.3 Stimulated Brillouin Scattering . . . . . 5

1.4 The Korteweg-de Vries (KdV) Equation . . . . . 8

1.5 Motivation . . . . . 9

2 THEORETICAL MODEL 10

2.1 Introduction . . . . . 10

2.2 Derivation of the Electromagnetic Wave Equation . . . . . 10

2.3 Derivation of the Driven KdV Equation in Inhomogeneous Medium 12

a) Harmonic Decomposition of the Driven KdV Equation . . . . 17

3 THE DRIVEN KDV EQUATION: LOCAL RESULTS 20

3.1 Introduction . . . . . 20

3.2 Comparison of the Driven KdV Equation with the Two Harmonic Model . . . . . 22

3.3 Autoresonance . . . . . 26

4 THE COUPLED KDV-ELECTROMAGNETIC WAVE EQUATIONS: RESULTS 36

4.1 Introduction . . . . . 36

4.2 Three Wave Model of SBS in Inhomogeneous Plasmas . . . . . 40

4.3 Results of Numerical Simulations . . . . . 42

5 SUMMARY AND CONCLUSION 57

BIBLIOGRAPHY 60

APPENDICES: 63

A NUMERICAL CONSIDERATIONS 63

B THE EQUIVALENCE OF THE DENSITY AND VELOCITY GRADIENTS IN THE LOCAL APPROXIMATION 65

# LIST OF FIGURES


1.1 *Mechanical analog of a parametric instability. The rod rotates at a frequency of* $\omega_0$*, causing the pendulum to change its length. The system becomes unstable if* $\omega_0 = 2\omega_1$*, since the amplitude of the pendulum will grow resonantly.* . . . . . 4

1.2 *Symbolic representation of the parametric instability in a plasma.* . . 6

3.1 *3-D Plot of the parameter space for* $h = 0.2$*,* $x = L/2$*, and* $x_0 = -75$*. The surfaces* a *to* d *correspond to: dispersion, damping, nonlinearity, and the velocity gradient respectively, they are defined in Eqs. (3.2) to (3.5). The smaller the perturbation required to reach the surface the more important the effect will be. The velocity gradient far from resonance saturates first,* d*, and is most important near the boundaries. Near the resonance point the velocity gradient is not important. If we assume small* $k$ *and large* $P$*, we see that the nonlinear term,* c*, will dominate. Dispersion,* a*, not surprisingly, is only important for large* $k$*, while the importance of damping,* b*, depends on its strength and the location in the parameter space.* . . . . . 23

3.2 *2-D cross-sections of the parameter space. Curve* a *corresponds to dispersion,* b *is defined by damping, and* c *describes nonlinear effects. Plot* A *shows the linear parameter space for P=0.00003, and* $\gamma_0$ *=0.0117. Plot* B *is the same except that P has been increased a factor of 10. Plot* C *is for P=0.0002, and* $\gamma_0$ *=0.03 and plot* D *for P=0.0002, and* $\gamma_0$ *=0.0117.* . . . . . 24

3.3 *KdV solution for* $h = 0$*, P=0.0002,* $k_A = 0.21$*, and* $x_0$*=-75.* . . . . . 25

3.4 *KdV solution for* $P = 0.00005$, $h = 0.3$, $k_A = 0.21$, *and* $x_0 = -75$. . . 27

3.5 *Two harmonic solution for 3.4* . . . . . 27

3.6 *KdV solution for* $P = 0.0002$, $h = 0.3$, $k_A = 0.21$, *and* $x_0 = -75$. . . . 28

3.7 *Two harmonic solution for 3.6.* . . . . . 28

3.8 *First harmonic for Fig. 3.7.* . . . . . 29

3.9 *Second harmonic for Fig. 3.7.* . . . . . 29

3.10 *Autoresonance curve: The curves between* ab *and* de *are unstable and cannot in reality be observed. A wave travelling from the left will climb the upper branch till it reaches either* a *or* b *at which point it will jump to branch* c*, likewise for the negative branch. A wave travelling from the right can jump only at point* d*, likewise for the positive branch. The parameters chosen are:* $x_0 = -8000$, $k_A = 0.32$, $L = 18000$, $h = 0.1$, $P = 0.00016$, *and* $\gamma_0 = 0.003$. . . . . 32

3.11 *Autoresonance curve: Two Harmonics. The parameters are the same as those in Fig. 3.10.* . . . . . 33

3.12 *Autoresonance curve: KdV. The parameters are the same as those in Fig. 3.10.* . . . . . 33

3.13 *Overlap of Figs. 3.10, 3.11, and 3.12. The discrepancy between Figs. 3.11 and 3.12 is clearly visible, even for small values of* $x$*, and is due to the stationary approximation used in the two harmonic approximation.* 34

4.1 *Comparison between the reflectivity observed from the KdV equation, (dotted line), and the reflectivity predicted by by Eq. (4.33), (solid line). The parameters chosen are* $h = 0.2$, $\gamma_0 = 0.0117$, *and* $P_0 = 0.03$. 43

4.2 *The reflectivity in the case of strong damping, for the parameters:* $h = 0$, $\gamma_0 = 0.08$, *and* $P_0 = 0.03$. . . . . 44

4.3 *The reflectivity, for the parameters:* $h = 0$, $\gamma_0 = 0.0117$, *and* $P_0 = 0.03$. 45

4.4 *Density at* $T = 8196$, *for the parameters shown in Fig. 4.3.* . . . . . 45

4.5 *Fourier transform of the density, for the parameters shown in Fig. 4.3.* 46

4.6 *Electric field amplitude at* $T = 8196$, *for the parameters shown in Fig. 4.3.* . . . . . 46

4.7 *Comparison between reflectivities obtained from the homogeneous and inhomogeneous plasmas. The dashed line is for conditions given in Fig. 4.3 for* $h = 0$, *the dotted line corresponds to* $h = 0.2$, *while the dot dashed line is Eq. (4.33) and the solid is Eq. (4.23). Notice that the gradient has lowered the average reflectivity, but it is not that dramatic. A more detailed picture of the early time development was shown in Fig. 4.1.* . . . . . 49

4.8 *The electric field at* $T = 3000$, *at the mid point of absolute growth. The parameters chosen are* $h = 0.2$, $\gamma_0 = 0.0117$, *and* $P_0 = 0.03$. . . . . 50

4.9 *Density at* $T = 3000$, *at the mid point of absolute growth, for the parameters shown in Fig. 4.8.* . . . . . 50

4.10 *Comparison between the homogeneous and inhomogeneous reflectivities for long times of Fig. 4.7. The upper line is for the conditions in Fig 4.3, while the lower line was Fig. 4.7, (dotted line).* . . . . . 51

4.11 *Electric Field at* $T = 4096$, *for the parameters shown in Fig. 4.8.* . . 52

4.12 *Density at* $T = 4096$, *for the parameters shown in Fig. 4.8.* . . . . . 52

4.13 *Electric Field at* $T = 5000$, *for the parameters shown in Fig. 4.8.* . . 53

4.14 *Density at $T = 5000$, for the parameters shown in Fig. 4.8.* . . . . . 53

4.15 *Electric Field at $T = 6144$, for the parameters shown in Fig. 4.8.* . . 54

4.16 *Density at $T = 6144$, for the parameters shown in Fig. 4.8.* . . . . . 54

4.17 *Frequency spectrum of the reflected light from a homogeneous plasma, for the reflectivity shown in Fig. 4.3.* . . . . . 55

4.18 *Frequency spectrum of the reflected light from an inhomogeneous plasma, for the reflectivity shown in Fig. 4.7, (dotted line). The broadening of the frequency spectrum is due to the continuum of resonance points, the apparent discreetness is due to the finite resolution.* . . . . . 55

4.19 *Comparison of reflectivity from the KdV electromagnetic wave equations, Eqs. (4.1) and (4.2), for various values of h at selected times. The top row of repeated symbols corresponds to average value of the reflectivity for large times, while the bottom row is the average value of the reflectivity taken at the saturation of the Rosenbluth stage, which is defined by Eq. (4.33).* . . . . . 56

A.1 *Schematic representation of the simulation box* . . . . . 64

# LIST OF IMPORTANT SYMBOLS AND DEFINITIONS

| | |
|---|---|
| SBS | Stimulated Brillouin scattering |
| SRS | Stimulated Raman scattering |
| $(\omega_0, k_0)$ | Laser pump frequency and wave vector |
| $(\omega_{0_b}, k_{0_b})$ | Scattered light frequency and wave vector |
| $(\omega_A, k_A)$ | Ion acoustic frequency and wave vector |
| $e$ | Electron charge |
| $Z$ | Atomic number |
| $c$ | Speed of light |
| $L$ | Length of the plasma |
| $m_\alpha$ | Electron $\alpha = e$ and ion $\alpha = i$ mass |
| $T_\alpha$ | Electron $\alpha = e$ and ion $\alpha = i$ temperature |
| $n_\alpha$ | Electron $\alpha = e$ and ion $\alpha = i$ density |
| $n_{0_\alpha}$ | Background electron $\alpha = e$ and ion $\alpha = i$ density |
| $n_c = \omega_0^2 m_e / 4\pi e^2$ | Critical density |
| $\gamma_0$ | Landau damping constant |
| $v_{th} = \sqrt{T_e/m_e}$ | Electron thermal speed |

| | |
|---|---|
| $\lambda_D = (T_e/4\pi e^2 n_{0_e})^{\frac{1}{2}}$ | Debye wave length |
| $k_D = 1/\lambda_D$ | Debye wave vector |
| $k_0 = (v_{th}/c)(\frac{n_e}{n_{0_e}} - 1)^{\frac{1}{2}} k_D$ | Pump wave vector |
| $\omega_{p_i} = (4\pi Z e^2 n_{0_i}/m_i)^{\frac{1}{2}}$ | Ion plasma frequency |
| $\omega_{p_e} = (4\pi e^2 n_{0_e}/m_e)^{\frac{1}{2}}$ | Electron plasma frequency |
| $[x] = \lambda_D$ | Unit of length |
| $[t] = 1/\omega_{p_i}$ | Unit of time |
| $N$ | Dimensionless ion plasma density |
| $\delta n = n_i(x)/n_{0_i} - 1$ | Ion density fluctuations |
| $b_n$ | The $n^{th}$ ion density harmonic amplitude |
| $c_A^0 = \sqrt{ZT_e/m_i}$ | Sound speed |
| $c_A(x) = c_A^0(1 + V(x))$ | Doppler shifted sound speed |
| $V(x) = h(x - x_0)/L$ | Inhomogeneous plasma flow speed |
| $h$ | Inhomogeneous flow strength |
| $x_0$ | Point of zero flow |
| $x_n = x_0 + Ln^2 k_A^2/2h$ | Coordinate of resonance point for $n^{th}$ harmonic |
| $V_0$ | Speed of reference frame |

| | |
|---|---|
| $\gamma_n = n\gamma_0 k_A$ | Damping on $n^{th}$ harmonic |
| $\Phi$ | Normalized electrostatic potential |
| $U$ | Fluid velocity |
| $E$ | Electric Field |
| $v_{osc} = eE/\omega_0 m_e$ | Quiver velocity amplitude |
| $a$ | Complex electromagnetic amplitude |
| $P$ | Fixed pondermotive amplitude |
| $P_0/2 = \mid a \mid^2 = v_{osc}^2/4v_{th}^2 = 2P/k_A$ | Intensity of the electric field at $x = 0$ |
| $R(t) = \mid a_0(x=0) \mid / \mid a_{0_b}(x=0) \mid$ | Reflectivity |
| $\mu_3 = 1/2(n_{0_e} m_i/n_c Z m_e)^{\frac{1}{2}}$ | Coupling constant |
| $V_{g_0}$ | Group velocity of electromagnetic wave |
| $G_0 = (v_{osc}^2 n_{0_e}/4v_{th}^2 n_c)(k_0 L/\gamma_0(1 - \frac{n_{0_e}}{n_c}))$ | Homogeneous gain |
| $G_g = (\pi v_{osc}^2 n_{0_e}/4v_{th}^2 n_c)(k_0 L/h(1 - \frac{n_{0_e}}{n_c}))$ | Inhomogeneous gain |
| $\Gamma_0 = (1/2\sqrt{2}) k_0^{\frac{1}{2}} v_{osc} \omega_{p_i}/\sqrt{\omega_0 c_A}$ | Convective growth rate of SBS |
| $\Gamma_{abs} = \left(\frac{2\Gamma_0}{\sqrt{V_{g_0}}}\left(1 - \frac{\pi^{\frac{1}{2}}}{G_g^{\frac{1}{2}}}\right) - \frac{\gamma_0 k_A}{c_A}\right)\frac{V_{g_0}}{V_{g_0}+c_A}$ | Absolute growth rate of SBS |

# CHAPTER ONE

# INTRODUCTION TO LASER PLASMA PHYSICS

## 1.1 Introduction

Plasma physics [1]-[5] is the study of ionized gases, which are often called the fourth state of matter due to the unique properties of such systems. Plasmas differ from ordinary gases in that the long range of the Coulomb potential allows for collective effects. Quasineutrality is an important characteristics of plasmas. The entire plasma is neutral, yet small scale local charge separation may occur. This local charge density provides a source for the electric field, which extends over the characteristic length, called the Debye length, $\lambda_D = (T_e/4\pi e^2 n_{0_e})^{\frac{1}{2}}$, where $e$ is the electric charge, $n_{0_e}$ is the electron number density, and $T_e$ is the electron temperature. The screening of the electric field over the distance $\lambda_D$, which effectively limits the range of a Coulomb interaction, is an example of a collective process. A large number of particles are required in the Debye sphere, $N_D = \frac{4\pi}{3} n_{0_e} \lambda_D^3$, for this to occur. When $N_D \gg 1$ the plasma exhibits fluid like behavior at the kinetic level. The dynamical evolution of electrons and ions is influenced by the mean field created by all the particles with a negligible influence from correlation between discrete particles i.e. two body collisions. The above properties are often considered as part of the definition of classical plasmas, which must satisfy:

$$N_D \gg 1 \tag{1.1}$$

and should extend over a characteristic length $L_0$

$$\lambda_D \ll L_0. \tag{1.2}$$

Unmagnetized plasmas [6], [7] can support three linear eigenmodes: ion-acoustic, Langmuir, and electromagnetic waves. The two electrostatic eigenmodes have the following dispersion relations:

$$\omega_A^2 = c_s^2 k^2. \tag{1.3}$$

$$\omega_L^2 = \omega_{p_e}^2 + 3v_{th}^2 k^2 \tag{1.4}$$

where $c_s = \left(\left(ZT_e + 3T_i\right)/m_i\right)^{\frac{1}{2}}$ are the sound speed, $T_e, T_i$ is the electron and ion temperatures respectively, $Z$ is the ion charge, $m_e, m_i$ are the electron and ion masses respectively, $\omega_{p_e} = \left(4\pi e^2 n_{0_e}/m_e\right)^{\frac{1}{2}}$ is the electron plasma frequency and $v_{th} = \left(T_e/m_e\right)^{\frac{1}{2}}$ is the electron thermal velocity. Equation (1.3) represents the low frequency ion acoustic waves and Eq. (1.4) represents the high frequency electron plasma wave or Langmuir wave. The acoustic mode is just a 'pressure' wave where the 'pressure' is partly exerted by the electric field instead of collisions. The electromagnetic wave's dispersion relation has the form:

$$\omega^2 = \omega_{p_e}^2 + c^2 k^2 \tag{1.5}$$

where $c$ is the speed of light.

Electrostatic waves and charged particles interact in a plasma. This interaction results in Landau damping [1], a collisionless process where particles and waves exchange energy. Particles whose phase velocity is slightly slower than that of the wave will interact with it, somewhat analogous to that of a surfer. The wave will 'catch' the particle and push it along and be damped in the process. A particle that is moving slightly faster will have the opposite effect on the wave and will lose its energy and enhance the wave. When the particles have a Maxwellian velocity distribution, $f_M$, there are more slower particles than faster, relative to the phase velocity of the wave, which leads to a net damping. The Landau damping parameter, $\gamma_L$, has the following mathematical form in Fourier space [3]:

$$\gamma_L = \frac{\pi}{2}\frac{\omega^3}{k^2}\frac{\partial f_M}{\partial v}\Big|_{\frac{\omega}{k}} \tag{1.6}$$

The general expression of Eq. (1.6) takes the following form for ion acoustic waves:

$$\gamma_L(k) = \sqrt{\frac{\pi}{8}\left(1+\frac{3}{\theta}\right)}\left\{\sqrt{\frac{Zm_e}{m_i}} + \theta^{\frac{3}{2}} exp\left(-\frac{\theta+3}{2}\right)\right\} kc_A = \gamma_0 k \qquad (1.7)$$

where $\theta = ZT_e/T_i$. The two terms on the right hand side of Eq. (1.7) correspond to electron and ion Landau damping respectively.

## 1.2 Parametric Instabilities

Laser plasma physics deals with the interaction of intense laser pulses with matter. In our studies the laser beam is simply treated as an energy source for the creation and heating of plasmas. Laser plasma physics has application in many areas, such as laser fusion, generation of x-rays, beat-wave particle acceleration schemes, diagnostic in magnetically confined plasmas and basic studies of turbulence.

The laser beam introduces free energy into the plasma, which can result in many instabilities. One important class of these interactions is known as parametric instabilities [3], [5], [7]. A mechanical analog of this instability, a driven pendulum, is shown in Fig. 1.1. The rotating rod changes the length of the pendulum in a periodic manner. When the frequency of the driver is exactly twice the frequency of pendulum, the system will be in resonance, and the small oscillation of the pendulum will start to grow. Mathematically this condition is:

$$\omega_0 = 2\omega_1. \qquad (1.8)$$

where $\omega_1$ is the frequency of the pendulum, and $\omega_0$ is the frequency of the rotating rod or driver. The pendulum system can gain energy only if friction can be overcome.

Small amplitude oscillations in a plasma vary in time but also propagate in space, so that a more accurate representation of parametric instability [8], [9] in a plasma would be the three wave coupling process. For example an electromagnetic

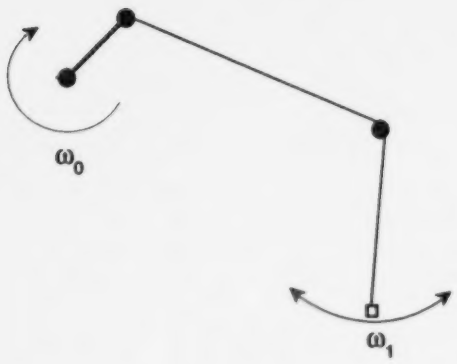


Figure 1.1: *Mechanical analog of a parametric instability. The rod rotates at a frequency of* $\omega_0$*, causing the pendulum to change its length. The system becomes unstable if* $\omega_0 = 2\omega_1$*, since the amplitude of the pendulum will grow resonantly.*

pump wave, $(\omega_0, \vec{k}_0)$ can play the role of the driver which decays into two daughter waves. The three modes which participate in this nonlinear interaction are characterized by the linear dispersion relation Eq. (1.3), (1.4), or (1.5) and satisfy the following matching conditions:

$$\omega_0 = \omega_1 + \omega_2, \tag{1.9}$$

$$\vec{k}_0 = \vec{k}_1 + \vec{k}_2, \tag{1.10}$$

where $(\vec{k}_0, \omega_0)$, $(\vec{k}_1, \omega_1)$, $(\vec{k}_2, \omega_2)$ are the wave number and frequency of the pump and two daughter waves, respectively. Equations (1.11)-(1.14) show possible matching conditions, which correspond to the most common parametric instabilities, where Eq. (1.11) desribes the parametric decay instability and Eq. (1.12) corresponds to two plasmon decay,

$$\omega_L = \omega_A + \omega_L{}' \tag{1.11}$$

$$\omega_0 = \omega_L + \omega_L{}' \tag{1.12}$$

Stimulated scattering instabilities are represented by:

$$\omega_0 = \omega_L + \omega_0', \tag{1.13}$$

$$\omega_0 = \omega_A + \omega_0', \tag{1.14}$$

where Eq. (1.13) corresponds to stimulated Raman scattering, (SRS), and Eq. (1.14) describes stimulated Brillouin scattering, (SBS). Instabilities in three wave interaction processes manifest themselves as a transfer of energy from the pump wave into daughter waves. The feedback loop, for the scattering instability SBS (1.14), is shown in Fig. 1.2. The growth of the density perturbation, $\delta n$, from the noise level leads to a transverse current, $\delta n v_0$, due to the coupling between the density perturbations $\delta n$, and the electron quiver velocity amplitude $v_0$, see Fig. 1.2. The oscillatory or quiver motion of the electrons results from the interaction with the transverse electric field of an electromagnetic wave. This transverse current is the source for the reflected electromagnetic wave which produces electron oscillations with a quiver velocity $v_{0_b}$. Finally the original density perturbations are enhanced by the ponderomotive force which is proportional to $v_0 v_{0_b}$.

## 1.3 Stimulated Brillouin Scattering

SBS [10], [11] corresponds to the decay of the pump wave into a backscattered electromagnetic wave and an ion acoustic wave [5] as shown in Eq. (1.14). This three wave interaction process is most effective where the following matching conditions are satisfied:

$$k_0 = k_{0_b} + k_A \tag{1.15}$$

$$\omega_0 = \omega_{0_b} + \omega_A \tag{1.16}$$

where $(k_0, \omega_0)$, $(k_{0_b}, \omega_{0_b})$, $(k_A, \omega_A)$ are the wave number and frequency, of the pump, backscattered radiation and ion-acoustic waves, respectively. Our discussion is lim-

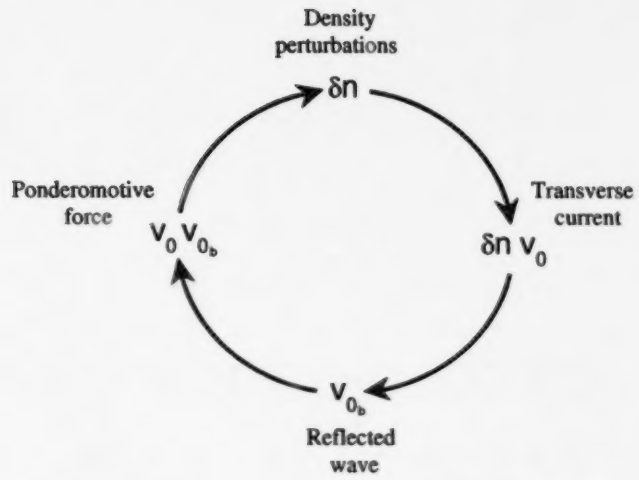


Figure 1.2: *Symbolic representation of the parametric instability in a plasma.*

ited to the backscattered SBS, which is a one-dimensional (1-D) process. The large difference between the electromagnetic and the ion-acoustic wave frequencies leads to an approximation of Eq. (1.16) as $\omega_0 \simeq \omega_{0_b}$. This allows us to combine the electromagnetic wave vectors in Eq. (1.15), and with the use of Eq. (1.5):

$$k_A \simeq 2k_0 = \frac{2v_{th}}{c}\sqrt{1 - \frac{n_{0_e}}{n_c}}. \tag{1.17}$$

where $n_c = \omega_0^2 m_e / 4\pi e^2$ is the critical electron density above which the electromagnetic wave with frequency $\omega_0$ cannot freely propagate in the plasma. Note that Eqs. (1.15) to (1.17) also imply that $k_{0_b} \simeq -k_0$.

The matching conditions of Eqs. (1.15) and (1.16) are satisfied everywhere in a homogeneous plasma. Consider however a more realistic case of an inhomogeneous plasma, which expands with a flow velocity $V(x) < c_A^0$. The local, Doppler shifted sound velocity, $c_A(x) = c_A^0 + V(x)$, defines the linear dispersion relation

$$\omega_A = c_A(x) k_A(x) \tag{1.18}$$

where the wave number $k_A(x)$ varies in space for a given constant ion-acoustic frequency. In such plasmas the matching conditions (1.15) and (1.16) have different solutions $\omega_{0_s}$, and $\omega_A$ at different points along the flow velocity profile $V(x)$, yielding a continuum of resonance points. Every resonance point in the inhomogeneous plasma corresponds to a well defined scattered electromagnetic wave and ion mode, satisfying the resonance conditions, Eqs. (1.15) and (1.16). For the simplified local model of Ch. 3, where we fix both the frequency $\omega_0 - \omega_{0_s}$ and wave number $k_0 - k_{0_s}$ of the driving ponderomotive force, the ion response is characterized by a single resonance point, unless we account for the nonlinear shift of the ion acoustic frequency which can broaden the resonance region.

SBS [6],[12]-[14] has been a difficult process to study because of its large parameter space and nonlinear behavior. The standard three wave interaction model of SBS [5] in a finite homogeneous plasma is a poor approximation to reality. This model along with most others predicts a saturated reflectivity close to 100% which differs from experimental results by at least a factor of 10. Experimentalists predict a value of SBS reflectivity of about a few percent.

The backscattered SBS is essentially a 1-D problem, however in reality the stimulated scattering can occur in all spatial directions. Several 2-D and 3-D studies have shown, that for a relatively narrow beam the interaction is dominated by backscattered SBS with negligible amount of side scattered and forward SBS. For example in Ref. [16] the results of a nonlinear homogeneous 1-D model, the type of model used in the present study, have agreed with 2-D simulations for the instability along the laser beam axis. Similar agreement has been observed in studies with a Gaussian pump [17] in 2-D.

## 1.4 The Korteweg-de Vries (KdV) Equation

The KdV [3], [4], [15], [18], [19] equation is used to model nonlinear ion-acoustic waves. Originally it was derived by two Dutch scientist studying the propagation of water waves in one direction in a shallow canal in 1895 [18]. The KdV equation reappeared 50 years later in the important numerical study of a nonlinear system by Fermi, Pasta, and Ulam [19]. The results of this numerical experiment had important implication for modern ergodic theory. The KdV equation now appears in the study of many diverse physical processes, from solid state physics to fluid dynamics to plasma physics. Zabusky and Kruskal in 1965 [20] numerically found its most well known solution, the soliton. Solitons may appear as a single hump or dent which vanishes at infinity, and possess the property that they do not lose their shape when colliding with one another. The KdV equation in plasmas has the following form:

$$\frac{\partial N}{\partial t} + c_A \frac{\partial N}{\partial x} + \frac{N}{2}\frac{\partial N}{\partial x} + \frac{1}{2}\frac{\partial^3 N}{\partial x^3} = 0, \tag{1.19}$$

where $N$ is the plasma density disturbance and $c_A$ is a constant sound speed. The first two terms are simply a propagation equation, the third is the nonlinear wave steepening term and the fourth is the dispersive term, due to charge neutrality violation. The soliton is produced by the balance of the nonlinear and dispersive terms. The driven KdV equation has the right hand side nonzero and as such can not be solved analytically using inverse scattering methods or the Bäcklund transformation [15]. When the source is periodic, harmonic decomposition can be used to approximate the KdV equation with a pair of coupled ordinary differential equations, (see the end of Ch. 2.3.a).

## 1.5 Motivation

The KdV equation was first coupled to the electromagnetic wave equation in [24]. I intend to extend this work by adding an inhomogeneous flow which will alter the ion-acoustic speed. This addition would improve the model another step, and bring it closer to experimental conditions [21]. The introduction of a flow velocity will allow many new regions of interest to be studied. The flow gradient would limit the size of the interaction region and thereby should limit the growth of the sound waves and reduce the reflectivity due to scattering instabilities. The balance between the flow gradient and nonlinear term will also allow us to study the process of autoresonance [23], [22].

This thesis is organized in the following way. Chapter 2 introduces a theoretical model. It shows derivations of an electromagnetic wave equation and the modified KdV equation, which contains an inhomogeneous flow velocity and nonlinear driver. Chapter 3 presents a local analysis of the driven KdV equation, where the driver models a constant amplitude periodic ponderomotive force. This equation is solved using harmonic decomposition. We have also discussed in Chapter 3 the autoresonance phenomenon. Chapter 4 presents numerical and analytical solutions to the full system of KdV electromagnetic wave equations in an inhomogeneous plasma. We have recovered the well known solution by Rosenbluth in the linear regime. New results for the nonlinear regime are presented.

# CHAPTER TWO

# THEORETICAL MODEL

## 2.1 Introduction

The purpose of this chapter is to introduce the basic equations for the physical processes discussed in this thesis. We will develope a theoretical model of stimulated Brillouin scattering in inhomogeneous plasmas. First the electrodynamic wave equation is derived from Maxwell's equations, next the driven KdV equation in an inhomogeneous medium is derived from the fluid equations and Poisson's equation. The driven KdV equation with a fixed amplitude driver, which is discussed in Ch. 3, and its harmonic decomposition [24], [25], [26], [27] is also shown.

## 2.2 Derivation of the Electromagnetic Wave Equation

We wish to model plasma perturbations caused by an intense laser beam interacting with an inhomogeneous expanding plasma. The laser beam will be modeled [12] by using the electromagnetic wave equation

$$\frac{1}{c^2}\frac{\partial^2 A}{\partial t^2} - \frac{\partial^2 A}{\partial x^2} = -\frac{4\pi}{c}J \tag{2.1}$$

where $A$ is the vector potential normal to the direction of wave propagation $x$, $c$ is the speed of light, $J$ is the current density, and we have chosen the Coulomb gauge. Ignoring thermal effects, we may use the conservation of canonical momentum to solve for the normal component of the electron velocity

$$v_\perp = \frac{eA}{m_e c}. \tag{2.2}$$

We assume a pump wave vector of the form $\vec{k}_0 = k_0\hat{e}_x$. Remembering that $J = n_e(x)ev_\perp$, with $n_e(x)$ the number density, we can use Eqs. (2.1) and (2.2) to get

$$\frac{1}{c^2}\frac{\partial^2 A}{\partial t^2} - \frac{\partial^2 A}{\partial x^2} = -\frac{4\pi e^2}{m_e c^2} n_e(x) A. \tag{2.3}$$

Using the electron plasma frequency, $\omega_{p_e}^2 = 4\pi e^2 n_{0_e}/m_e$, Eq. (2.3) can be rewritten as:

$$\frac{1}{c^2}\frac{\partial^2 A}{\partial t^2} - \frac{\partial^2 A}{\partial x^2} = -\frac{\omega_{p_e}^2}{c^2}\left(1 + \left(\frac{n_e(x)}{n_{0_e}} - 1\right)\right) A. \tag{2.4}$$

The high frequency variations of the electromagnetic field can be explicitly accounted for by writing $A = \hat{a}\, e^{-i\omega_0 t} + \hat{a}^*\, e^{i\omega_0 t}$, where $\omega_0$ is the laser frequency and $\hat{a}$ is a slowly varing in the vector potential amplitude. Dropping the small second order time derivative of $\hat{a}$, Eq. (2.4) now has the form:

$$-i2\omega_0\frac{\partial \hat{a}}{\partial t} - \omega_0^2\hat{a} - c^2\frac{\partial^2 \hat{a}}{\partial x^2} = -\omega_{p_e}^2\,\hat{a} - \omega_{p_e}^2\,\hat{a}\left(\frac{n_e(x)}{n_{0_e}} - 1\right) \tag{2.5}$$

Defining $a{=}\hat{a}e/2c\sqrt{mT_e}$ as the dimesionless vector potential amplitude, Eq. (2.5) may be rewritten as:

$$i2\frac{\omega_0\omega_{p_e}}{\omega_{p_i}}\frac{c_A^0}{v_{th}}\frac{\partial a}{\partial t} + \left(\frac{\lambda_D\omega_{p_e}}{v_{th}}c\right)^2\frac{\partial^2 a}{\partial x^2} + \left(\omega_0^2 - \omega_{p_e}^2\right)a = \omega_{p_e}^2\, a\left(\frac{n_e(x)}{n_{0_e}} - 1\right) \tag{2.6}$$

where $\omega_{p_i} = (4\pi Z e^2 n_{0_e}/m_i)^{\frac{1}{2}}$ is the ion plasma frequency, $\sqrt{T_e/m_e}$ is the electron thermal velocity, $\lambda_D = (T_e/4\pi e^2 n_{0_e})^{\frac{1}{2}}$ is the Debye length, and $c_A^0 = \lambda_D\omega_{p_i}$. Introducing normalized quantities, which will be used from now on, $[t]{=}1/\omega_{p_i}$ and $[x]{=}\lambda_D$, Eq. (2.6) becomes,

$$i\frac{\partial a}{\partial t} + \mu_1\frac{\partial^2 a}{\partial x^2} + \mu_2 a = \mu_3 a\left(\frac{n_e(x)}{n_{0_e}} - 1\right) \tag{2.7}$$

where the constants $\mu_1 = \mu_3 c^2/v_{th}^2$, $\mu_2 = \mu_1 k_0^2/k_D^2$, and $\mu_3 = 1/2(n_{0_e}m_i/n_c Z m_e)^{\frac{1}{2}}$, $k_0^2 = (v_{th}^2/c^2)\,(n_c/n_{0_e} - 1)$ is the pump wave vector in the plasma, and $n_c = \omega_0^2 m_e/4\pi e^2$ is the critical density.

In the electromagnetic wave equation charge seperation can be neglected. This allows us to set $en_e = -Zen_i$, so Eq. (2.7) becomes:

$$i\frac{\partial a}{\partial t} + \mu_1 \frac{\partial^2 a}{\partial x^2} + \mu_2 a = \mu_3 a \delta n \tag{2.8}$$

where we defined $\delta n = (n_i(x)/n_{0_i} - 1)$.

## 2.3 Derivation of the Driven KdV Equation in Inhomogeneous Medium

The Korteweg-de Vries equation [24] describes the propagation of ion-acoustic waves in a plasma. In order to model realistic properties of ion-accoustic waves additional terms must be added to the KdV equation such as Landau damping, inhomogeneous flow and a driver. The deriviation begins from the following system of plasma fluid equations [3], [28]:

$$\frac{\partial N}{\partial t} + \frac{\partial (NU)}{\partial x} = 0 \tag{2.9}$$

$$\frac{\partial U}{\partial t} + U\frac{\partial U}{\partial x} = -\frac{\partial \Phi}{\partial x} - \Gamma_{th}\frac{\partial (\ln N)}{\partial x} \tag{2.10}$$

and Poisson's equation

$$\frac{\partial^2 \Phi}{\partial x^2} = n_0 \exp(\Phi - P) - N. \tag{2.11}$$

where $U$ is the fluid velocity in units of $c_A^0$, $N$ is the dimensionless ion plasma density, $\Gamma_{th} = 3T_i/ZT_e$ is a small thermal correction, $\Phi$ is the dimensionless electrostatic potential, and $P{=}|a|^2$ the dimensionless ponderomotive potential term. The variables have been normalized as such: $a{=}\hat{a}e/2c\sqrt{mT_e}$ the vector potential, and $\Phi{=}\hat{\Phi}e/T_e$ the electrostatic potential. Equation (2.9) is the continuity equation and represents the conservation of particles. The Navier Stokes equation, (2.10), has an additional electrostatic force term. The second term on the right hand side of Eq. (2.10), represents a correction for thermal pressure. In Poissons's equation, (2.11), the electron density

is represented by a Boltzman distribution, and $P$ is the ponderomotive potential produced by the laser beam. To derive the KdV equation we will switch to a reference frame moving with the wave

$$x' = k_A x - \omega_A t, \quad t' = \omega_A t \tag{2.12}$$

where $\omega_A = k_A(1 + V_0)$ and $V_0$ is the actual expansion velocity at a reference point in the plasma. In these new coordinates the spatial and temporal derivatives become:

$$\frac{\partial}{\partial x} = k_A \frac{\partial}{\partial x'}, \qquad \frac{\partial}{\partial t} = \omega_A(\frac{\partial}{\partial t'} - \frac{\partial}{\partial x'}). \tag{2.13}$$

Equations (2.9)-(2.11) now have the form:

$$\omega_A(\frac{\partial N}{\partial t'} - \frac{\partial N}{\partial x'}) + k_A \frac{\partial (NU)}{\partial x'} = 0 \tag{2.14}$$

$$\omega_A(\frac{\partial U}{\partial t'} - \frac{\partial U}{\partial x'}) + k_A U \frac{\partial U}{\partial x'} = -k_A \frac{\partial \Phi}{\partial x'} - k_A \Gamma_{th} \frac{\partial (\ln N)}{\partial x'} \tag{2.15}$$

$$k_A{}^2 \frac{\partial^2 \Phi}{\partial x'^2} = n_0 \exp(\Phi - P) - N. \tag{2.16}$$

We assume that we have an inhomogenous expanding fluid where both $n_0(x)$ and $V(x)$ are known. The variables have the following perturbative expansion:

$$N = n_0 + \epsilon n^{(1)} + \epsilon^2 n^{(2)} + \cdots \tag{2.17}$$

$$U = V + \epsilon v^{(1)} + \epsilon^2 v^{(2)} + \cdots \tag{2.18}$$

$$\Phi = \epsilon \phi^{(1)} + \epsilon^2 \phi^{(2)} + \cdots \tag{2.19}$$

$$P = \epsilon^2 p^{(2)} + \cdots \tag{2.20}$$

where $n_0$, and $V$ are slowly varying functions of $x$. Substituting the expansions (2.17)-(2.20) into Eqs. (2.9) through (2.11) we get:

$$(1 + V_0)(\frac{\partial}{\partial t'} - \frac{\partial}{\partial x'})[n_0 + \epsilon n^{(1)} + \epsilon^2 n^{(2)} + \cdots] +$$

$$\frac{\partial}{\partial x'}[(n_0+\epsilon n^{(1)}+\epsilon^2 n^{(2)}+\cdots)(V+\epsilon v^{(1)}+\epsilon^2 v^{(2)}+\cdots)]=0 \tag{2.21}$$

$$(1+V_0)(\frac{\partial}{\partial t'}-\frac{\partial}{\partial x'})(V+\epsilon v^{(1)}+\epsilon^2 v^{(2)}+\cdots)+\frac{1}{2}\frac{\partial}{\partial x'}[V+\epsilon v^{(1)}+\epsilon^2 v^{(2)}+\cdots]^2=$$
$$-\frac{\partial}{\partial x'}(\epsilon\phi^{(1)}+\epsilon^2\phi^{(2)}+\cdots)-\Gamma_{th}\frac{\partial}{\partial x'}\ln(n_0+\epsilon n^{(1)}+\epsilon^2 n^{(2)}+\cdots) \tag{2.22}$$

$$k_A{}^2\frac{\partial^2}{\partial x'^2}(\epsilon\phi^{(1)}+\epsilon^2\phi^{(2)}+\cdots)=n_0\exp[(\epsilon\phi^{(1)}+\epsilon^2\phi^{(2)}+\cdots)-$$
$$(\epsilon^2 p^{(2)}+\cdots)]-(n_0+\epsilon n^{(1)}+\epsilon^2 n^{(2)}+\cdots) \tag{2.23}$$

Collecting terms of order $\epsilon$ and assuming that $\Gamma_{th}=\bigcirc(\epsilon)$ and $k_A^2=\bigcirc(\epsilon)$ while $\frac{\partial n^{(1)}}{\partial t'},\frac{\partial v^{(1)}}{\partial t'},\frac{\partial n_0}{\partial x'},\frac{\partial v}{\partial x'}=\bigcirc(\epsilon^2)$ the equations reduce to:

$$-(1+V_0)\frac{\partial n^{(1)}}{\partial x'}+n_0\frac{\partial v^{(1)}}{\partial x'}+V\frac{\partial n^{(1)}}{\partial x'}=0 \tag{2.24}$$

$$-(1+V_0)\frac{\partial v^{(1)}}{\partial x'}+V\frac{\partial v^{(1)}}{\partial x'}=-\frac{\partial\phi^{(1)}}{\partial x'} \tag{2.25}$$

$$n_0\phi^{(1)}-n^{(1)}=0. \tag{2.26}$$

Rearranging terms we have:

$$-\frac{\partial n^{(1)}}{\partial x'}+(V-V_0)\frac{\partial n^{(1)}}{\partial x'}+n_0\frac{\partial v^{(1)}}{\partial x'}=0 \tag{2.27}$$

$$-\frac{\partial v^{(1)}}{\partial x'}+(V-V_0)\frac{\partial v^{(1)}}{\partial x'}=-\frac{\partial\phi^{(1)}}{\partial x'} \tag{2.28}$$

$$n_0\phi^{(1)}-n^{(1)}=0. \tag{2.29}$$

If $V-V_0\simeq\bigcirc(\epsilon)$, i.e. the plasma expansion velocity $V(x)$ differs by a small amount from $V=V_0$ at the reference point, then

$$v^{(1)}=\phi^{(1)},\quad n^{(1)}=n_0v^{(1)}=n_0\phi^{(1)}=\delta n \tag{2.30}$$

where $\delta n=n_i(x)/n_{0_i}-1$. To second order in $\epsilon$ the Eqs. (2.21) to (2.23) reduce to:

$$(1+V_0)(\frac{\partial n^{(1)}}{\partial t'}-\frac{\partial n^{(2)}}{\partial x'})+n_0\frac{\partial v^{(2)}}{\partial x'}+V\frac{\partial n^{(2)}}{\partial x'}+\frac{\partial(v^{(1)}n^{(1)})}{\partial x'}+\Delta V\frac{\partial n^{(1)}}{\partial x'}+\frac{\partial(n_0V)}{\partial x'}=0 \tag{2.31}$$

$$(1+V_0)(\frac{\partial v^{(1)}}{\partial t'}-\frac{\partial v^{(2)}}{\partial x'})+\frac{1}{2}\left\{\frac{\partial V^2}{\partial x'}+2v^{(1)}\frac{\partial v^{(1)}}{\partial x'}+V\frac{\partial v^{(2)}}{\partial x'}\right\}+\Delta V\frac{\partial v^{(1)}}{\partial x'} =$$

$$-\frac{\partial \phi^{(2)}}{\partial x'}-\Gamma_{th}\frac{1}{n_0}\frac{\partial n^{(1)}}{\partial x'} \tag{2.32}$$

$$k_A{}^2\frac{\partial^2\phi^{(1)}}{\partial x'^2}=n_0\phi^{(2)}-n_0p^{(2)}+\frac{1}{2}n_0(\phi^{(1)})^2-n^{(2)} \tag{2.33}$$

where $\Delta V = V - V_0 \simeq \bigcirc(\epsilon)$. Regrouping the velocity terms we can drop terms proportional to $\bigcirc(\epsilon^3)$.

$$(1+V_0)\frac{\partial n^{(1)}}{\partial t'}-\frac{\partial n^{(2)}}{\partial x'}+n_0\frac{\partial v^{(2)}}{\partial x'}+\frac{\partial(v^{(1)}n^{(1)})}{\partial x'}+\Delta V\frac{\partial n^{(1)}}{\partial x'}+\frac{\partial(n_0V)}{\partial x'}=0 \tag{2.34}$$

$$(1+V_0)\frac{\partial v^{(1)}}{\partial t'}-\frac{\partial v^{(2)}}{\partial x'}+\frac{1}{2}\frac{\partial V^2}{\partial x'}+v^{(1)}\frac{\partial v^{(1)}}{\partial x'}+\Delta V\frac{\partial v^{(1)}}{\partial x'}=-\frac{\partial \phi^{(2)}}{\partial x'}-\Gamma_{th}\frac{1}{n_0}\frac{\partial n^{(1)}}{\partial x'} \tag{2.35}$$

$$k_A{}^2\frac{\partial^2\phi^{(1)}}{\partial x'^2}=n_0\phi^{(2)}-n_0p^{(2)}+\frac{1}{2}n_0(\phi^{(1)})^2-n^{(2)} \tag{2.36}$$

Substituting Eq. (2.30) into (2.34)-(2.36), our system becomes:

$$(1+V_0)\frac{\partial \delta n}{\partial t'}-\frac{\partial n^{(2)}}{\partial x'}+n_0\frac{\partial v^{(2)}}{\partial x'}+\frac{1}{2n_0}\frac{\partial(\delta n)^2}{\partial x'}+\Delta V\frac{\partial \delta n}{\partial x'}+\frac{\partial(n_0V)}{\partial x'}=0 \tag{2.37}$$

$$\frac{(1+V_0)}{n_0}\frac{\partial \delta n}{\partial t'}-\frac{\partial v^{(2)}}{\partial x'}+\frac{1}{2}\frac{\partial V^2}{\partial x'}+\frac{1}{n_0{}^2}\delta n\frac{\partial \delta n}{\partial x'}+\frac{\Delta V}{n_0}\frac{\partial \delta n}{\partial x'}=-\frac{\partial \phi^{(2)}}{\partial x'}-\Gamma_{th}\frac{1}{n_0}\frac{\partial \delta n}{\partial x'} \tag{2.38}$$

$$k_A{}^2\frac{\partial^2\delta n}{\partial x'^2}=n_0{}^2\phi^{(2)}-n_0{}^2p^{(2)}+\frac{1}{2}(\delta n)^2-n_0n^{(2)}. \tag{2.39}$$

Multiplying Eq. (2.38) by $n_0$ and adding (2.37) we get:

$$2(1+V_0)\frac{\partial \delta n}{\partial t'}-\frac{\partial n^{(2)}}{\partial x'}+\frac{1}{n_0}\frac{\partial(\delta n)^2}{\partial x'}+\frac{n_0}{2}\frac{\partial V^2}{\partial x'}+$$

$$2\Delta V\frac{\partial \delta n}{\partial x'}+\frac{\partial(n_0V)}{\partial x'}=-n_0\frac{\partial \phi^{(2)}}{\partial x'}-\Gamma_{th}\frac{\partial \delta n}{\partial x'} \tag{2.40}$$

and taking the partial derivative with respect to $x$, dividing by $n_0$ and keeping only terms of order $\epsilon^2$, Eq. (2.39) gives:

$$\frac{k_A{}^2}{n_0}\frac{\partial^3\delta n}{\partial x'^3}=n_0\frac{\partial \phi^{(2)}}{\partial x'}-n_0\frac{\partial p^{(2)}}{\partial x'}+\frac{1}{2n_0}\frac{\partial(\delta n)^2}{\partial x'}-\frac{\partial n^{(2)}}{\partial x'}. \tag{2.41}$$

Adding Eqs. (2.40) and (2.41), dividing by two and rearranging the terms produces:

$$(1+V_0)\frac{\partial \delta n}{\partial t'} + \frac{1}{2n_0}\frac{\partial (\delta n)^2}{\partial x'} + \frac{\Gamma_{th}}{2}\frac{\partial \delta n}{\partial x'} + \Delta V \frac{\partial \delta n}{\partial x'} + \frac{{k_A}^2}{2n_0}\frac{\partial^3 \delta n}{\partial {x'}^3} + \frac{1}{2}\frac{\partial (n_0 V)}{\partial x'} + \frac{n_0}{4}\frac{\partial V^2}{\partial x'} = -\frac{n_0}{2}\frac{\partial p^{(2)}}{\partial x'}. \tag{2.42}$$

Converting back to the lab frame,

$$\frac{\partial}{\partial t'} = \frac{1}{\omega_A}\frac{\partial}{\partial t} + \frac{1}{k_A}\frac{\partial}{\partial x}, \qquad \frac{\partial}{\partial x'} = \frac{1}{k_A}\frac{\partial}{\partial x} \tag{2.43}$$

our equation becomes:

$$\frac{(1+V_0)}{\omega_A}\frac{\partial \delta n}{\partial t} + \frac{(1+V_0)}{k_A}\frac{\partial \delta n}{\partial x} + \frac{1}{2k_A n_0}\frac{\partial (\delta n)^2}{\partial x} + \frac{\Gamma_{th}}{2k_A}\frac{\partial \delta n}{\partial x} + \frac{\Delta V}{k_A}\frac{\partial \delta n}{\partial x} + \frac{1}{2k_A n_0}\frac{\partial^3 \delta n}{\partial x^3} + \frac{1}{2k_A}\frac{\partial (n_0 V)}{\partial x} + \frac{n_0}{4k_A}\frac{\partial V^2}{\partial x} = -\frac{n_0}{2k_A}\frac{\partial p^{(2)}}{\partial x}. \tag{2.44}$$

Since $(1+V_0)k_A/\omega_A = 1$ we get:

$$\frac{\partial \delta n}{\partial t} + \frac{1}{2n_0}\frac{\partial (\delta n)^2}{\partial x} + (1+V_0)\frac{\partial \delta n}{\partial x} + \frac{\Gamma_{th}}{2}\frac{\partial \delta n}{\partial x} + \Delta V \frac{\partial \delta n}{\partial x} + \frac{{k_A}^2}{2n_0}\frac{\partial^3 \delta n}{\partial x^3} + \frac{1}{2}\frac{\partial (n_0 V)}{\partial x} + \frac{n_0}{4}\frac{\partial V^2}{\partial x} = -\frac{n_0}{2}\frac{\partial p^{(2)}}{\partial x}. \tag{2.45}$$

If we assume that $\frac{\partial V^2}{\partial x}$ and $\frac{\partial (n_0 V)}{\partial x}$ are $\ll \bigcirc(\epsilon^2)$ we arrive at the modified KdV equation:

$$\frac{\partial \delta n}{\partial t} + (1 + V + \frac{1}{2}\Gamma_{th})\frac{\partial \delta n}{\partial x} + \frac{1}{2n_0}\frac{\partial (\delta n)^2}{\partial x} + \frac{1}{2n_0}\frac{\partial^3 \delta n}{\partial x^3} = -\frac{n_0}{2}\frac{\partial p^{(2)}}{\partial x}. \tag{2.46}$$

This paper will concentrate on the case where density is homogeneous, $n_0 = 1$, see Appendix B, $\Gamma_{th} \simeq 0$, and $V(x)$ is a perturbation to the local sound speed. Since $p^{(2)} = |a|^2$ and after introducing linear Landau damping, the equation has the following form:

$$\frac{\partial \delta n}{\partial t} + \gamma \cdot \delta n + (1+V)\frac{\partial \delta n}{\partial x} + \frac{1}{2}\frac{\partial (\delta n)^2}{\partial x} + \frac{1}{2}\frac{\partial^3 \delta n}{\partial x^3} = -\frac{1}{2}\frac{\partial |a|^2}{\partial x}. \tag{2.47}$$

where $\gamma \cdot \delta n = \int \gamma_L(x-y)\delta n(y)dy$, and $\gamma_L(x-y)$ corresponds to the Landau damping term.

The set of coulped KdV electromagnetic wave equations have the following form:

$$i\frac{\partial a}{\partial t} + \mu_1 \frac{\partial^2 a}{\partial x^2} + \mu_2 a = \mu_3 a \delta n \tag{2.48}$$

$$\frac{\partial \delta n}{\partial t} + \gamma \cdot \delta n + (1 + V(x))\frac{\partial \delta n}{\partial x} + \frac{1}{2}\frac{\partial (\delta n)^2}{\partial x} + \frac{1}{2}\frac{\partial^3 \delta n}{\partial x^3} = -\frac{1}{2}\frac{\partial |a|^2}{\partial x}. \tag{2.49}$$

where Eq. (2.48) is (2.8) and Eq. (2.49) is (2.47). In the course of the derivation we have implicitly assumed that the value of $k_A \ll 1$ and the expansion velocity $V$ changes by a small amount in the plasma, $\mid V - V_0 \mid \ll 1$.

*a) Harmonic Decomposition of the Driven KdV Equation*

Solving Eqs. (2.48) and (2.49) is a computationally intensive process. The following decomposition will give us a simple but approximate method for obtaining stationary solutions, with little computational time. The harmonic decomposition will be applied to the local description of SBS, (cf. Ch. 3), which corresponds to the KdV equation with a constant amplitude driver varying in space and time as a linear sound wave. The driven KdV equation has the following form:

$$\frac{\partial \delta n}{\partial t} + \gamma \cdot \delta n + (1 + V(x))\frac{\partial \delta n}{\partial x} + \frac{1}{2}\frac{\partial (\delta n)^2}{\partial x} + \frac{1}{2}\frac{\partial^3 \delta n}{\partial x^3} = P\sin(k_A x - \omega_A t + \phi_0) \tag{2.50}$$

where $P$ is a constant, $\phi_0$ is an arbitrary phase constant and $V(x)$ is the expansion velocity. A transformation of variables will allow us to use harmonic decomposition. The new variables are:

$$\xi = x - \frac{\omega_A}{k_A} t \simeq x - t; \quad \eta = x, \tag{2.51}$$

where we have assumed that $\xi$ and $\eta$ are the fast and slowly varing variables respectively. The partial derivatives become:

$$\frac{\partial}{\partial t} = -\frac{\partial}{\partial \xi}, \qquad \frac{\partial}{\partial x} = \frac{\partial}{\partial \eta} + \frac{\partial}{\partial \xi}. \tag{2.52}$$

Thus Eq. (2.50) now has the following form:

$$\frac{\partial \delta\tilde{n}}{\partial \eta} + \gamma \cdot \delta\tilde{n} + V(\eta)\frac{\partial \delta\tilde{n}}{\partial \xi} + \frac{1}{2}\frac{\partial (\delta\tilde{n})^2}{\partial \xi} + \frac{1}{2}\frac{\partial^3 \delta\tilde{n}}{\partial \xi^3} = P\sin(k_A\xi) \tag{2.53}$$

where we have dropped the small term containing $V(x)\frac{\partial}{\partial \eta}$. The equation can be decomposed by using a stationary approximation:

$$\delta\tilde{n} = \sum_{|n|\geq 1} \tilde{b}_n(\eta)\exp(-ink_A\xi), \quad \tilde{b}_{-n} = \tilde{b}_n^*. \tag{2.54}$$

This harmonic decomposition results in:

$$\tilde{b}_n' + \gamma_n \cdot \tilde{b}_n + ik_A nV(\eta)\tilde{b}_n + \frac{ink_A}{2}\sum_{p\neq n} \tilde{b}_p\tilde{b}_{n-p} - \frac{i(nk_A)^3}{2}\tilde{b}_n = \frac{P}{2i}\delta_{n,1}, \tag{2.55}$$

where the $'$ represent a derivative with respect to $\eta$ and in Fourier space $\gamma_n = n\gamma_0 k_A$ where $\gamma_0$ is the Landau damping coefficient defined in Eq. (1.7). The first two harmonics satisfy the following equations:

$$\tilde{b}_1' + \gamma_1 \cdot \tilde{b}_1 + ik_A V(\eta)\tilde{b}_1 + ik_A\tilde{b}_1^*\tilde{b}_2 - \frac{ik_A^3}{2}\tilde{b}_1 = \frac{P}{2i} \tag{2.56}$$

$$\tilde{b}_2' + \gamma_2 \cdot \tilde{b}_2 + i2k_A V(\eta)\tilde{b}_2 + ik_A(\tilde{b}_1)^2 - i4k_A^3\tilde{b}_2 = 0. \tag{2.57}$$

where we have neglected higher order terms to truncate the infinite series. Renormalizing $\tilde{b}_1 = b_1/2i$ and rearranging terms, the Eqs. (2.56) and (2.57) become:

$$b_1' + \gamma_1 \cdot b_1 + ik_A(V(\eta) - \frac{k_A^2}{2})b_1 - ik_A b_1^* b_2 = P \tag{2.58}$$

$$b_2' + 2\gamma_1 \cdot b_2 + i2k_A(V(\eta) - 2k_A^2)b_2 - \frac{ik_A}{4}(b_1)^2 = 0. \tag{2.59}$$

The linear limit of Eq. (2.58) is just $b_2 = 0$. The above approximations are valid so long as $|b_3| \ll |b_1|$. Assuming that the spatial derivative is small we may solve for $b_3$, from Eq. (2.55), in terms of $b_2$ and $b_1$. These solutions have the following form:

$$a)\, b_3 = \frac{-i3k_A b_1 b_2}{\gamma_3 + i3k_A(V(\eta) - \frac{9}{2}k_A^2)}, \quad b)\, b_2 = \frac{ik_A(b_1)^2}{\gamma_2 + i2k_A(V(\eta) - 2k_A^2)}. \tag{2.60}$$

Substituting Eq. (2.60.b) into Eq. (2.60.a), dropping the $\gamma's$ with respect to $k_A$ and requiring that $|b_3| \ll |b_1|$, we get:

$$1 \gg \frac{|\, b_1 \,|^2}{2|(V(\eta) - \frac{9}{2}k_A^2)(V(\eta) - 2k_A^2)|}. \tag{2.61}$$

The two possible limits are:

$$a) V(\eta) \simeq 0 \qquad b) V(\eta) \not\simeq 0 \tag{2.62}$$

The limit (2.62.$a$), when substituded into Eq. (2.61), leads to the strong restriction of

$$|\, b_1 \,| \ll 3k_A^2. \tag{2.63}$$

Limit (2.62.$b$), when substituted into Eq. (2.61), imposes no new restrictions on $b_1$ since the density perturbations cannot become large outside of the resonant region. The inequality (2.63), for example, implies that the density perturbations, $\delta n \propto b_1$, must be kept below 7% for a value of $k_A$=0.21$k_D$ for the frequency shift approximation, [29], [30], to be valid. The frequency shift approximation can be obtained by substituding Eq. (2.60.$b$) into Eq. (2.58).

# CHAPTER THREE

# THE DRIVEN KDV EQUATION: LOCAL RESULTS

## 3.1 Introduction

The local model [28], [24] is an approximation to the coupled KdV-electromagnetic wave equations, (2.48) and (2.49). Nonlinear ion-acoustic waves vary on the spatial scale which is shorter than the wavelength of the linear sound waves. This is contrary to the variations of the ponderomotive force amplitude (the right side of Eq. (2.49)), which is nearly constant over several wavelengths. The local approximation takes advantage of this scale separation and replaces the driving term on the right hand side of the KdV equation (2.49) by a periodic force with a constant driver

$$\frac{\partial \delta n}{\partial t} + + \gamma \cdot \delta n + V(x)\frac{\partial \delta n}{\partial x} + \frac{1}{2}\frac{\partial (\delta n)^2}{\partial x} + \frac{1}{2}\frac{\partial^3 \delta n}{\partial x^3} = P\sin[k_A x - \omega_A t + \phi_0]. \qquad (3.1)$$

Equation (3.1) includes a damping term $\gamma \cdot \delta n = \int \gamma(x-y)\delta n(y)dy$, and the flow $V(x)$. The flow velocity will be chosen to be a linear function of $x$ defined as $V = h(x-x_0)/L$ where $L$ is the length of the box, and $h$ the dimensionless gradient parameter, which is assumed to be less than 1. Equation (3.1) describes the local response of the nonlinear sound waves to the periodic ponderomotive force, which varies in space and time as a plane linear sound wave, which satisfies the SBS matching conditions (1.15) and (1.16). The boundary and initial conditions are given in Appendix A, along with the physical parameters used, except as noted.

Each of the six terms on the left hand side of (3.1) originates from a different physical process and each can dominate in certain regions of the parameter space. The first two terms represent the propagation equation and are responsible for the

movement of the wavelets to the right with speed $c_A = 1$. The third term corresponds to Landau damping, which determines the maximum amplitude the perturbations may have at saturation. This result is obtained by dropping all the other terms on the left hand side, taking the maximum value of the driver, and solving for $\delta n$:

$$\delta n = \frac{P}{\gamma_L} = \frac{P}{\gamma_L(k_A)} \tag{3.2}$$

where the characteristic wavelength is defined by $k_A$ and $\gamma_L(k_A)=\gamma_0 k_A$, (1.7). The fourth term describes the effect of the inhomogeneous flow velocity, $V(x)$, and is responsible for the location of a resonance point. The inhomogeneous flow velocity limits the region of ion wave excitation. If the density is saturated by the inhomogeneous effects one obtains

$$\delta n = \frac{P}{k_A V(x)} = \frac{PL}{hk_A(x - x_0)}. \tag{3.3}$$

The importance of the above equation, for limiting the value of $\delta n$, is only away from the resonance point $x = x_0$. The fifth term represents nonlinearity, and is responsible for wave steepening. It can also saturate the plasma response by producing higher ion wave harmonics at $2k_A$, $3k_A$, etc. It gives the following limit on the maximum density perturbations

$$\delta n = \sqrt{\frac{P}{k_A}}. \tag{3.4}$$

The final term on the left hand side corresponds to ion sound wave dispersion. Its saturation equation takes the following form:

$$\delta n = \frac{2P}{k_A^3}. \tag{3.5}$$

A 3-D visual representation of Eqs. (3.2) to (3.5) is shown in Fig. 3.1, while selected 2-D slices are shown in Fig. 3.2. In the present examples we have discussed weakly damped sound waves $\gamma_L/\omega_A = \gamma_0 < 0.1$. By considering small linear Landau damping throughout this study, we emphasize the importance of nonlinear and inhomogeneous

effects on the saturation of SBS. In the stationary regime the amplitude $\delta n$ of the density perturbations varies with the wave number $k/k_D$. In particular, due to a strong dependance on the wave number, dispersive effects (3.5), (curve a in Fig. 3.2), are always the most important cause of saturation at large $k/k_D$ values. The nonlinear wave steeping (3.4), (curve $c$ in Fig. 3.2), is most effective in the saturation of SBS at small $k/k_D$ values, i.e. for long wavelength ion acoustic waves. Finally the level of saturation depends on the value of the driver's amplitude $P$. The saturation density levels are smaller at lower $P$, Fig.3.2 A and larger for larger $P$, Fig. 3.2 B. Different regimes of parameters discussed in Figs. 3.1 to 3.2, will help us in the interpretation of numerical results from the local simulations and from the full system of equations Eq. (2.48) and (2.49).

The solution to Eq. (3.1), for the homogeneous plasma ($h = 0$), is shown in Fig. 3.3. The increasing part of the density profile at the left hand side is due to Landau damping, since the perturbation starts from zero. The parameters chosen in Fig. 3.3 are the same as those in Fig. 3.2 D, where for a value of $k_A = 0.21k_D$ the lowest curve, c, which describes nonlinear effects, should saturate the instability at about $\delta n \sim 0.05$, (cf. Fig. 3.3). The slight asymmetry in $\delta n$ shown in Fig. 3.3 implies that we are in a weakly nonlinear regime.

## 3.2 Comparison of the Driven KdV Equation with the Two Harmonic Model

The reduction of the partial differential KdV equation into a coupled set of first order ordinary differential equations is an interesting result in itself, since the reduction in computational time is dramatic, hours versus minutes. The two harmonic approximation is shown to be in good agreement with the KdV equation. In Ch. 2 we found the two harmonic approximation [25], [26], Eqs. (2.58) and (2.59):

$$b_1' + \gamma_1 b_1 + ik_A(V - \frac{k_A^2}{2})b_1 - ik_A b_1^* b_2 = P \tag{3.6}$$

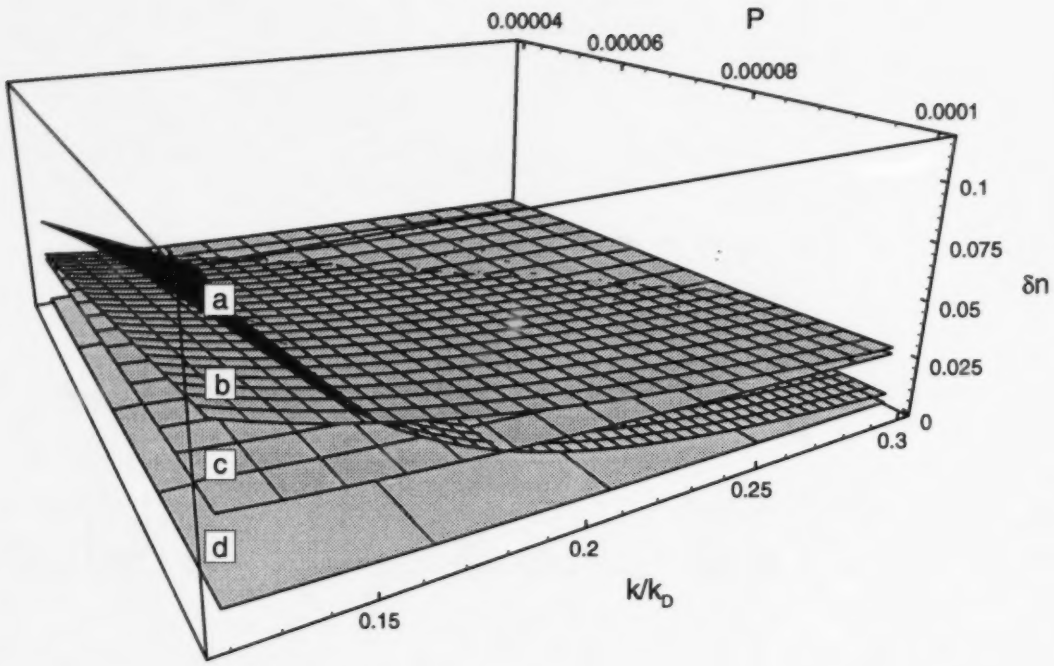


Figure 3.1: *3-D Plot of the parameter space for* $h = 0.2$, $x = L/2$, *and* $x_0 = -75$. *The surfaces* a *to* d *correspond to: dispersion, damping, nonlinearity, and the velocity gradient respectively, they are defined in Eqs. (3.2) to (3.5). The smaller the perturbation required to reach the surface the more important the effect will be. The velocity gradient far from resonance saturates first,* d, *and is most important near the boundaries. Near the resonance point the velocity gradient is not important. If we assume small* $k$ *and large* $P$, *we see that the nonlinear term,* c, *will dominate. Dispersion,* a, *not surprisingly, is only important for large* $k$, *while the importance of damping,* b, *depends on its strength and the location in the parameter space.*

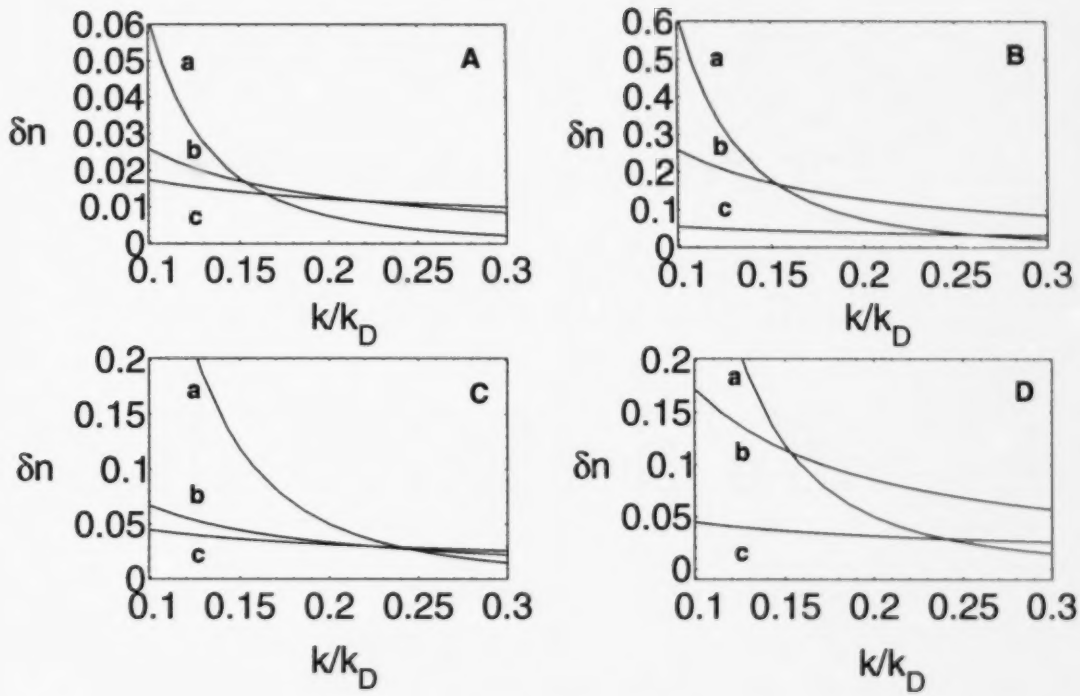


Figure 3.2: *2-D cross-sections of the parameter space. Curve* a *corresponds to dispersion,* b *is defined by damping, and* c *describes nonlinear effects. Plot* A *shows the linear parameter space for P=0.00003, and* $\gamma_0$ *=0.0117. Plot* B *is the same except that P has been increased a factor of 10. Plot* C *is for P=0.0002, and* $\gamma_0$ *=0.03 and plot* D *for P=0.0002, and* $\gamma_0$ *=0.0117.*

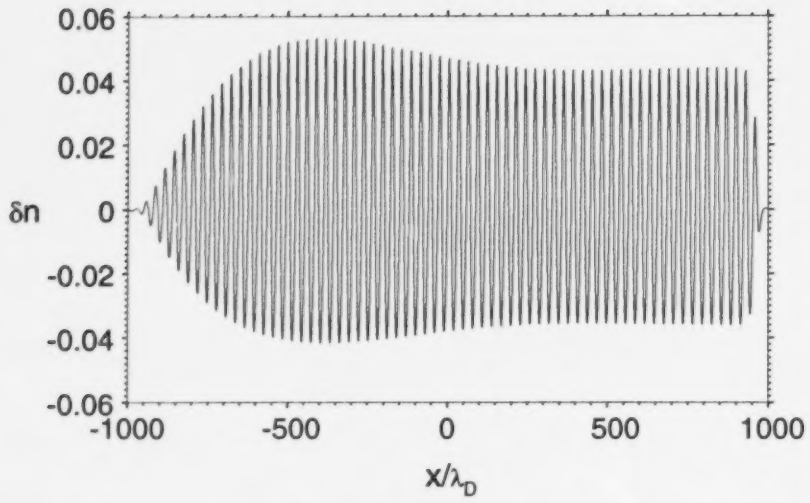


Figure 3.3: *KdV solution for* $h = 0$, *P=0.0002,* $k_A = 0.21$, *and* $x_0$=*-75.*

$$b_2' + 2\gamma_1 b_2 + i2k_A(V - 2k_A^2)b_2 - \frac{ik_A}{4}(b_1)^2 = 0. \tag{3.7}$$

for the KdV equation where $\eta$ has been replaced by $x$ with the use of Eq. (2.51). To recover $\delta n$ from these equations we use Eq. (2.54). This leads to:

$$\delta n = Im(b_1 \exp(ik_A(x-t)) + 2ib_2 \exp(i2k_A(x-t))) \tag{3.8}$$

where the factor of $2i$ is due to the normalization chosen earlier. The Eqs. (3.6) and (3.7) each posses a resonant point for their respective harmonic, defined as:

$$x_1 = x_o + \frac{Lk_A^2}{2h}, \quad x_2 = x_o + \frac{2Lk_A^2}{h}, \tag{3.9}$$

for the first and second harmonic respectively. Each wavelet moves with speed $c_A = 1$ inside the envelope.

Figure 3.4 shows the full KdV solution in a nearly linear regime. The resonance region corresponds to the large broad peak. The secondary peaks are due to phase

modulations produced by the gradient. The two harmonic solution is shown in Fig. 3.5 and reproduces the general features of the KdV equation quite well. The point of exact resonance, Eq. (3.9), for $b_1$ occurs at $x_1 = x_0 + Lk_A^2/2h$=72, likewise $x_2 = x_0 + 2Lk_A^2/h$=513, $x_0$=-75. The convective term, $\frac{\partial \delta n}{\partial x}$ in Eq. (3.1) or $b_1'$ in Eq. (3.6), is responsible for the shift of the peak position to the right of the resonance point. The small perturbation of the resonance peak is the result of the second harmonic which has disturbed the symmetric first harmonic.

The nonlinear solution showed that the second harmonic is responsible not only for the asymmetry but also the phase mismatch in the right side of Fig. 3.6. The degree of mismatch depends on the nonlinearity and the actual location of the second harmonic resonance, Eq. (3.9). Comparing Figs. 3.6 and 3.7 shows the good agreement between the KdV solution and the two harmonic solution. The main peak in the KdV solution is slightly broader and smoother than the two harmonic solution due to the influence of higher harmonics and dispersion. The saturation response predicted by Fig. 3.2 D curve c is nonlinear, as the asymmetry in $\delta n$ implies. Figure. 3.8 and 3.9 show the shapes of the first and second harmonic respectively. The peak of the second harmonic occurs to the right of the maximum of the first harmonic because it is driven by the first. This is because the amplitude of the first harmonic is usual small near the resonant point of the second harmonic and so the maximum of the second harmonic occurs before its resonance point. Notice that the first and second harmonics are symmetric but their sum is not.

## 3.3 Autoresonance

Autoresonance [22], [23] is the effect related to a balance between the nonlinear and gradient terms which produces an extended resonant region where the perturbations can grow. As discussed in Ch. 3.1, inhomogeneous and nonlinear effects can separately contribute to the saturation of the density response by creating a mismatch between

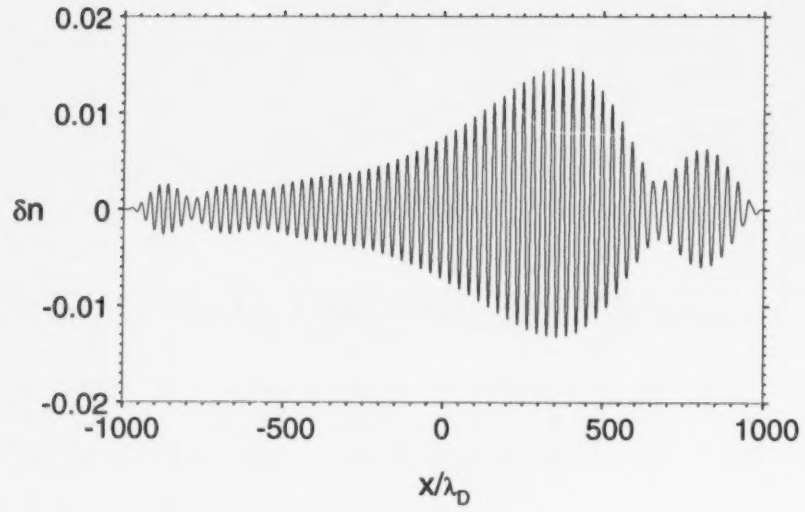


Figure 3.4: *KdV solution for* $P = 0.00005$, $h = 0.3$, $k_A = 0.21$, *and* $x_0 = -75$.

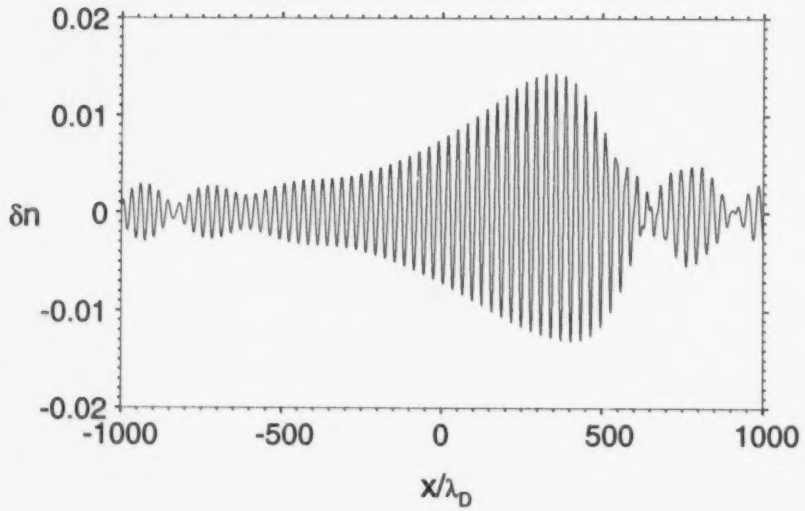


Figure 3.5: *Two harmonic solution for 3.4*

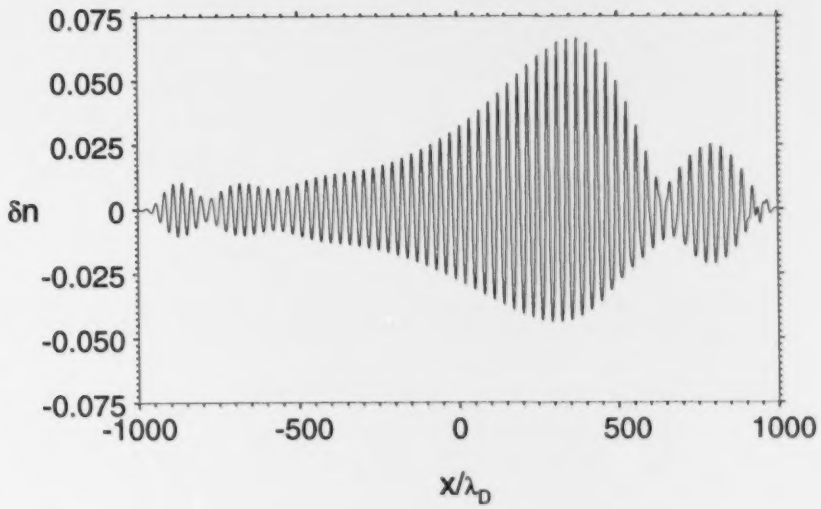


Figure 3.6: *KdV solution for* $P = 0.0002$, $h = 0.3$, $k_A = 0.21$, *and* $x_0 = -75$.

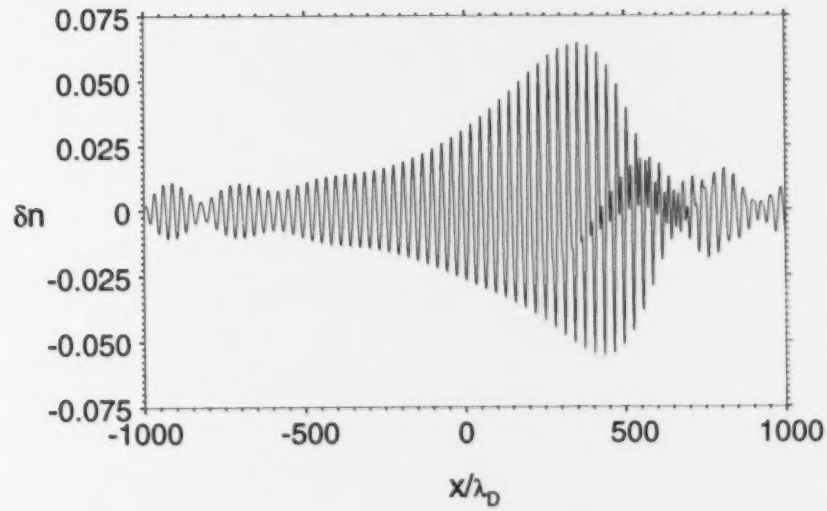


Figure 3.7: *Two harmonic solution for 3.6.*

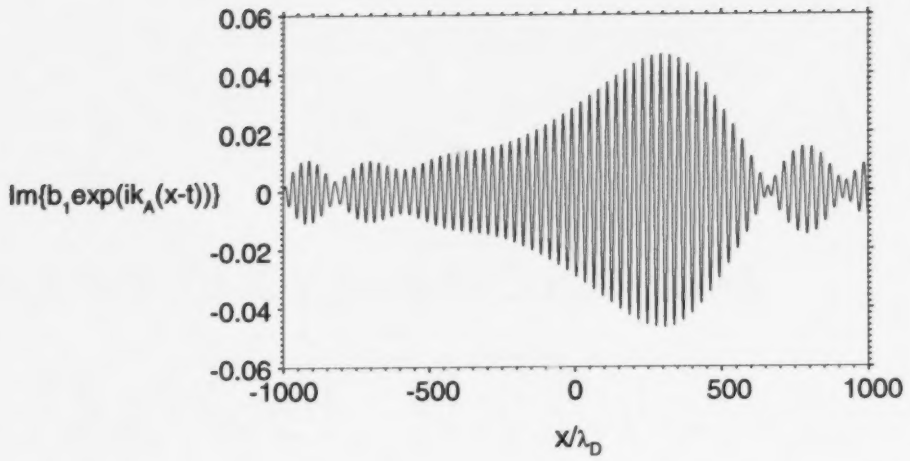


Figure 3.8: *First harmonic for Fig. 3.7.*

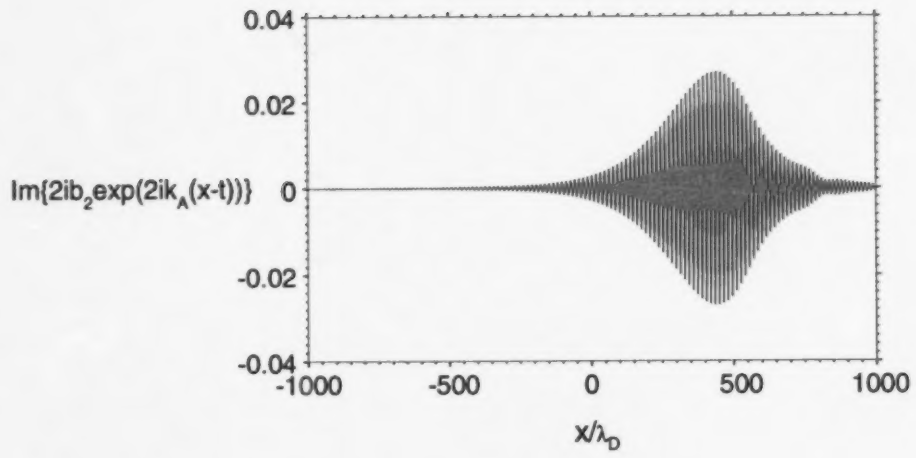


Figure 3.9: *Second harmonic for Fig. 3.7.*

the driver and the resonant sound wave. However, it is possible, as pointed out by Friedland [22], for the nonlinear frequency shift to balance the mismatch created by an inhomogeneous flow velocity. This cancellation effect extends the resonance region and can contribute to the enhancement of ion acoustic waves. We will examine this process within the framework of a KdV equation. This model is more general than the original studies of Friedland [22] and Friedland and Kaufman [23], which were based on the simple frequency shift approximation.

The two harmonic approximation used in Eqs. (2.58) and (2.59) allows us to reduce autoresonance to a simple mathematical formula. Consider Eqs. (2.58) and (2.59), with damping and the convective derivative dropped from the second equation

$$b_1' + \gamma_1 b_1 + ik_A(V - \frac{k_A^2}{2})b_1 - ik_A b_1^* b_2 = P \tag{3.10}$$

$$i2k_A(V - 2k_A^2)b_2 - \frac{ik_A}{4}(b_1)^2 = 0 \tag{3.11}$$

where we remember that $\gamma_1 = \gamma_0 k_A$ and $\mid b_2 \mid \ll \mid b_1 \mid$. This approximation allows us to combine Eq. (3.10) and (3.11) to produce the frequency shift equation [29], [30] for $b_1$:

$$b_1' + \gamma_1 b_1 + ik_A(V - \frac{k_A^2}{2})b_1 - \frac{ik_A^2 \mid b_1 \mid^2 b_1}{4(2k_A(V - \frac{k_A^2}{2}) - 3k_A^3)} = P. \tag{3.12}$$

The maximum density fluctuations occur near the resonance point $V - k_A^2/2$ and so in the nonlinear term we may drop $2k_A(V - k_A^2/2)$ with respect to $3k_A^3$, this leaves

$$b_1' + \gamma_1 b_1 + ik_A(V - \frac{k_A^2}{2})b_1 + \frac{i \mid b_1 \mid^2 b_1}{12k_A} = P. \tag{3.13}$$

We can rewrite $b_1 = B(x)\exp(i\phi(x))$, where both $B$ and $\phi$ are real. Equation (3.13) decomposes into its real and imaginary parts as follows

$$B' + \gamma_1 B = P cos(\phi). \tag{3.14}$$

$$B\phi' + k_A(V - \frac{k_A^2}{2})B + \frac{B^3}{12k_A} = -P\sin(\phi). \tag{3.15}$$

Assuming that a stationary solution exists and that damping is strong enough so that we are rapidly attracted to it, we may drop the derivatives, eliminate $\phi$, and with $V = h(x - x_0)/L$, we obtain for $x$

$$x = x_0 + \frac{k_A^2 L}{2h} + \frac{L}{h}\left\{ -\frac{B^2}{12k_A^2} \pm \sqrt{\frac{P^2}{k_A^2 B^2} - \frac{\gamma_1^2}{k_A^2}} \right\}. \tag{3.16}$$

An autoresonance condition is defined as $x_0 + k_A^2 L/2h - B^2 L/(12hk_A^2) \approx 0$, i.e. a balance between the inhomogeneous flow and nonlinear terms. Notice that $x = x(B^2)$ so the result is symmetric with respect to the x-axis. Fig. 3.10 shows a typical example of autoresonance, note that $B \propto b_1 \propto \delta n$ by Eq. (3.8). The function becomes triple valued between **ab** and **de** which indicates that an unstable solution may exist. The top branch shows the possible paths of a right going wave. By reaching point **a** along the upper branch, the amplitude of a sound wave is affected by the autoresonance process. The bottom branch shows the only path a left travelling wave can take. The usual resonance would have predicted a single valued symmetric curve.

Discrepancies between solutions to the harmonic equations (3.6) and (3.7), Fig 3.11, and the KdV equation (3.1) shown in Fig. 3.12 start at small values of $x$ and for low amplitude sound waves. We associate this disagreement with the stationary approximation used in the harmonic decomposition model. The driven KdV equation contains full spatial and temporal evolution of sound waves and leads to the solution, Fig. 3.13, which shows a transition from the upper branch to point **b**, (Fig. 3.10), at large sound wave amplitudes. The apparent lack of autoresonance effects in the KdV solution could be related to the stability of the full solution, which follows a single valued dependance on $x$ in Fig. 3.10.

Finally we would also like to comment on the region of validity of the autoresonance phenomena, as it was originally proposed by Friedland [22],[23]. Based on the harmonic approximation, Eqs. (3.6) and (3.7), we have found that autoresonance can only occur in an extremely narrow region in the parameter space. Defining

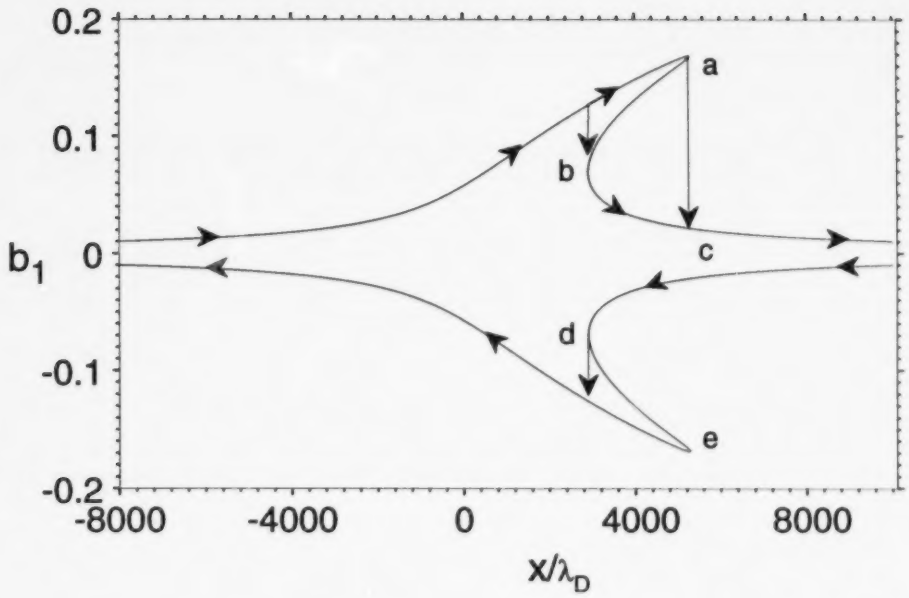


Figure 3.10: *Autoresonance curve: The curves between* ab *and* de *are unstable and cannot in reality be observed. A wave travelling from the left will climb the upper branch till it reaches either* a *or* b *at which point it will jump to branch* c*, likewise for the negative branch. A wave travelling from the right can jump only at point* d*, likewise for the positive branch. The parameters chosen are:* $x_0 = -8000$, $k_A = 0.32$, $L = 18000$, $h = 0.1$, $P = 0.00016$, *and* $\gamma_0 = 0.003$.

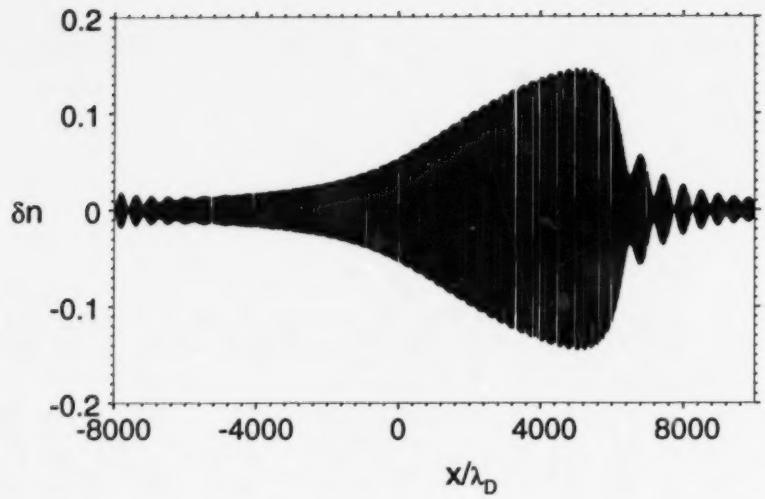


Figure 3.11: *Autoresonance curve: Two Harmonics. The parameters are the same as those in Fig. 3.10.*

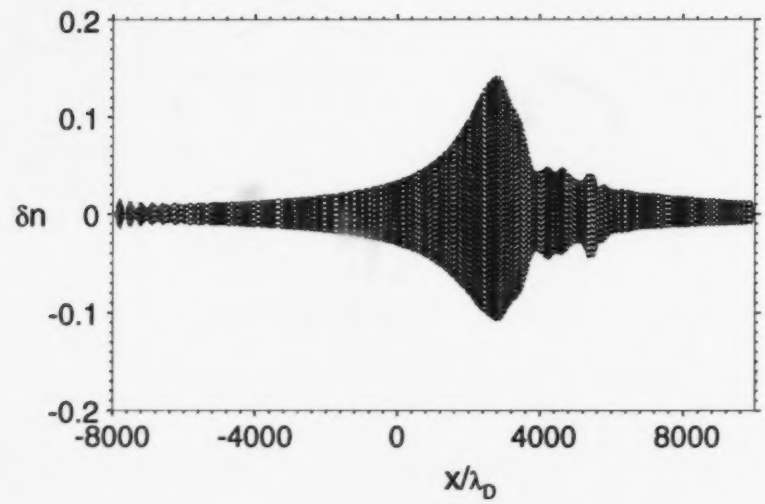


Figure 3.12: *Autoresonance curve: KdV. The parameters are the same as those in Fig. 3.10.*

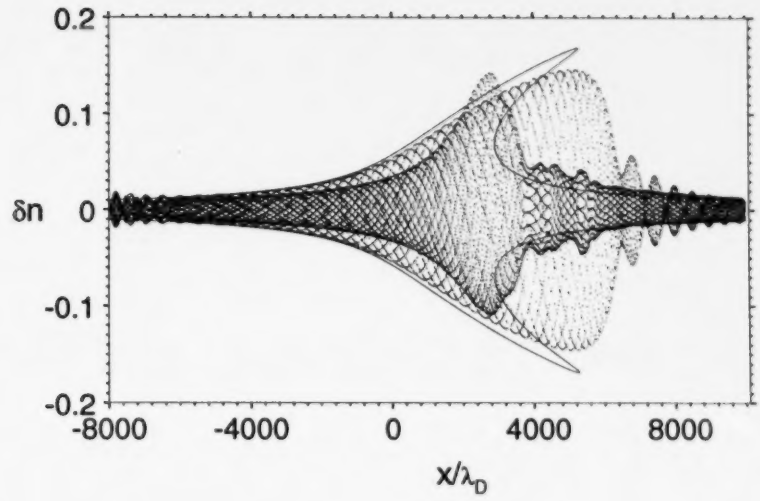


Figure 3.13: *Overlap of Figs. 3.10, 3.11, and 3.12. The discrepancy between Figs. 3.11 and 3.12 is clearly visible, even for small values of $x$, and is due to the stationary approximation used in the two harmonic approximation.*

$\xi = \sqrt{k_A h}(x - x_0 - Lk_A^2/2h)/L$ as a dimensionless length, Eq. (3.16) reduces to

$$\xi = -\frac{B^2}{12k_A}\sqrt{\frac{L}{k_A h}} \pm \sqrt{\left(\frac{P}{B}\sqrt{\frac{L}{k_A h}}\right)^2 - \left(\gamma_1\sqrt{\frac{L}{k_A h}}\right)^2}. \tag{3.17}$$

Our first assumption was that we are rapidly attracted to our solution or:

$$\gamma_1\sqrt{\frac{L}{k_A h}}B \gg \left|\frac{dB}{d\xi}\right|. \tag{3.18}$$

Remembering that $dB/d\xi = (d\xi/dB)^{-1}$ and assuming that $B \ll P/\gamma_1$ we obtain:

$$\gamma_1 \gg \frac{k_A h}{L}\left(\frac{-B^2}{6k_A} \pm \frac{P}{B}\right)^{-1}. \tag{3.19}$$

Since we always have to satisfy the inequality, even at its maximum, we want to find the maximum value for the right hand side. Setting the first derivative equal to zero and evaluating the function at that point we get

$$\gamma_1 \gg \left(\frac{L}{k_A h}\right)^{-1}\left(\frac{P^2}{3k_A}\right)^{-\frac{1}{3}} \tag{3.20}$$

where we have dropped the small numerical factor. The second condition states that we must be able to see the phenomena which requires that points a and b or similarly d and e in Fig. 3.10, must be widely spaced. Near point a, $\xi_{max} = (12k_A)^{-1}\sqrt{L/k_A h}(P/\gamma_1)^2$ which is Eq. (3.17) evaluated at its maximum value of $P/\gamma_1$. At point b $\xi$ is just the right hand side of Eq. (3.19) evaluated at the maximum which is $\xi_b = 3/2\left((L/k_A h)^{\frac{3}{2}} P^2/6k_A\right)^{\frac{1}{3}}$, therefore we have:

$$(12k_A)^{-1}\sqrt{\frac{L}{k_A h}}\left(\frac{P}{\gamma_1}\right)^2 \gg \frac{3}{2}\left(\left(\frac{L}{k_A h}\right)^{\frac{3}{2}}\frac{P^2}{6k_A}\right)^{\frac{1}{3}}. \tag{3.21}$$

The above reduces to a form which is independent of $h$,

$$\gamma_1 \ll 3^{-\frac{1}{2}}\left(\frac{P^2}{6k_A}\right)^{\frac{1}{3}}. \tag{3.22}$$

Summarizing, the three conditions required for autoresonance to occur are:

$$\gamma_1 \gg \frac{L}{h}\left(\frac{3k_A}{P^2}\right)^{\frac{1}{3}}; \quad \gamma_1 > \frac{P}{3k_A^2}; \quad \gamma_1 \ll 3^{-\frac{1}{2}}\left(\frac{P^2}{6k_A}\right)^{\frac{1}{3}} \tag{3.23}$$

where the first condition requires that damping be strong enough to give the quasistationary solution. The second condition makes sure that the frequency shift equation itself remains valid, see Eq. (2.63). The final condition represents the requirement that the region between b and c is large enough so that the effect is noticeable. Notice that there is an upper and a lower limit on damping and this region is rather narrow. Autoresonance was not found in a region that is considered physically relevant. To get the effect it was necessary to reduce Landau damping to $\gamma_L/\omega_A = \gamma_0 = 0.003$, or three tenths of electron Landau damping. The minimum electron Landau damping rate predicted by Eq. (1.7), for $ZT_e/T_i \to \infty$, is $\sqrt{\pi Z m_e/8m_i}k$=$0.01k$.

# CHAPTER FOUR

# THE COUPLED KDV-ELECTROMAGNETIC WAVE EQUATIONS: RESULTS

## 4.1 Introduction

The numerical solution to the coupled KdV-electromagnetic wave equation, with an inhomogeneous plasma flow term, will now be presented. In Ch. 3 we have analyzed solutions to the driven KdV equation where the reflected light and pump wave were 'fixed', and represented in terms of a constant amplitude periodic driver. SBS now evolves in time and space from a small seed. The dimensionless KdV-electromagnetic wave equations were derived in Ch. 2 as (2.48) and (2.49), they are:

$$i\frac{\partial a}{\partial t} + \mu_1 \frac{\partial^2 a}{\partial x^2} + \mu_2 a = \mu_3 a \delta n, \tag{4.1}$$

$$\frac{\partial \delta n}{\partial t} + \gamma \cdot \delta n + \left(1 + \frac{h}{L}(x - x_0)\right)\frac{\partial \delta n}{\partial x} + \frac{1}{2}\frac{\partial (\delta n)^2}{\partial x} + \frac{1}{2}\frac{\partial^3 \delta n}{\partial x^3} = -\frac{1}{2}\frac{\partial |a|^2}{\partial x}, \tag{4.2}$$

where $\gamma \cdot \delta n = \int \gamma(x-y)\delta n(y)dy$ is the linear Landau damping term (1.7), $h$ is the dimensionless gradient strength, $L$ is the length of the box, $x_0$ is the point of zero flow velocity, $\mu_1 = \mu_3 c^2/v_{th}^2$, $\mu_2 = \mu_1 k_0^2/k_D^2$, and $\mu_3 = (1/2)(n_{0_e} m_i/n_e Z m_e)^{\frac{1}{2}}$. The boundary and initial conditions are given in Appendix A, along with the physical parameters used.

Linear growth of SBS occurs in two distinct ways: absolute or convective. Absolutely unstable modes grow in time at every point inside the box. Convective or spatially growing modes increase their amplitude during propagation. A density disturbance in a given point in the box will start to grow as the unstable perturbation approaches, and then once the wave has passed, will start to decay because of damping. To obtain the growth rates and thresholds for SBS we will solve a homogeneous

linear dispersion relation. Neglecting nonlinear and the flow terms in the evolution of the sound waves in Eq. (4.2) we obtain:

$$i\frac{\partial a}{\partial t} + \mu_1 \frac{\partial^2 a}{\partial x^2} + \mu_2 a = \mu_3 a \delta n, \tag{4.3}$$

$$\frac{\partial \delta n}{\partial t} + \gamma_0 k_A \delta n + \frac{\partial \delta n}{\partial x} = -\frac{1}{2}\frac{\partial |a|^2}{\partial x}. \tag{4.4}$$

We further simplify Eqs. (4.3) and (4.4) by introducing three resonant SBS modes: an electromagnetic pump wave and backscattered radiation,

$$a = \bar{a}_0 \exp(ik_0 x) + \bar{a}_{0_b} \exp(i(k_{0_b} x - (\omega_{0_b} - \omega_0)t)) + c.c. \tag{4.5}$$

and an ion-acoustic wave,

$$\delta n = \delta \bar{n} \exp(i(k_A x - \omega_A t)) + c.c. \tag{4.6}$$

where *c.c.* stands for complex conjugate. Assuming that the amplitudes, $\bar{a}_{0_b} and \delta \bar{n}$, vary slowly in space and time we may drop their higher order derivatives. The matching conditions, Eqs. (1.15) and (1.16) along with Eq. (1.17), allow us to equate $\omega_{0_b} - \omega_0$ and $\omega_A$, and approximate $k_A$ by $2k_0$ and $k_{0_b}$ by $-k_0$. With the above solutions and gathering terms with like powers, Eqs. (4.3) and (4.4) become:

$$i\frac{\partial \bar{a}_{0_b}}{\partial t} - i\mu_1 k_A \frac{\partial \bar{a}_{0_b}}{\partial x} = \mu_3 \bar{a}_0 \delta \bar{n}^* \tag{4.7}$$

$$\frac{\partial \delta \bar{n}}{\partial t} + \gamma_0 k_A \delta \bar{n} + \frac{\partial \delta \bar{n}}{\partial x} = \frac{-i}{2} k_A \bar{a}_0 \bar{a}^*_{0_b}. \tag{4.8}$$

where we have replaced $\gamma_L(k_A)$ by $\gamma_0 k_A$ from Eq. (1.7). Letting $\mu_1 k_A = c^2 k_0/\omega_0 c_A = V_{g_0}/c_A$ where $V_{g_0}$ represents the group velocity of the reflected SBS wave and $\mu_3 = (1/2)\omega_{p_e} v_{th}/\omega_0 c_A$. Renormalizing $A_1 = i\bar{a}_{0_b}/\sqrt{\bar{a}_0 \omega_{p_e} v_{th}/2\omega_0 c_A}$ and $A_2 = \delta \bar{n}^*/\sqrt{\bar{a}_0^* k_0/k_D}$ and taking the complex conjugate of Eq. (4.8) we arrive at

$$\frac{\partial A_1}{\partial t} - \frac{V_{g_0}}{c_A}\frac{\partial \bar{A}_1}{\partial x} = \Gamma_0 A_2 \tag{4.9}$$

$$\frac{\partial A_2}{\partial t} + \gamma_0 k_A A_2 + \frac{\partial A_2}{\partial x} = \Gamma_0 A_1 \tag{4.10}$$

where

$$\Gamma_0 = \frac{\omega_{p_i}}{2\sqrt{2}} \frac{v_{osc}}{v_{th}} \left( \frac{\omega_{p_e} v_{th} k_0}{\omega_0 c_A k_D} \right)^{\frac{1}{2}} = \frac{1}{2\sqrt{2}} \frac{k_0^{\frac{1}{2}} v_{osc} \omega_{p_i}}{\sqrt{\omega_0 c_A}} \tag{4.11}$$

and Eqs. (4.9) and (4.10) represent the standared parametric instability equations [5]. Introducing an ansatz $A_1 = \bar{A}_1 \exp(-i(kx - \omega t))$ and $A_2 = \bar{A}_2 \exp(-i(kx - \omega t))$ where we assume that $k$ is real and $\omega$ is complex will allow us to solve for the dispersion relation $D(k, \omega(k)) = 0$. The dispersion relation obtained from Eqs. (4.9) and (4.10) is

$$D(k, \omega(k)) = \left( \omega + \frac{V_{g_0}}{c_A} k \right) (\omega - k + i\gamma_0 k_A) + \Gamma_0^2 = 0 \tag{4.12}$$

For the system to be absolutely unstable [9] requires [31] that both $D(k, \omega) = 0$ and $\partial D(k, \omega)/\partial k = 0$. Using $\partial D(k, \omega)/\partial k = 0$ gives

$$k = \frac{c_A}{2V_{g_0}} \left( \omega \left( \frac{V_{g_0}}{c_A} - 1 \right) + i \frac{V_{g_0}}{c_A} \gamma_0 k_A \right). \tag{4.13}$$

Substituting Eq. (4.13) into Eq. (4.12) yields the frequency

$$\omega = -i \frac{V_{g_0} \gamma_0 k_A}{V_{g_0} + c_A} + \Gamma_0 \frac{2\sqrt{-V_{g_0} c_A}}{V_{g_0} + c_A} \tag{4.14}$$

which contains an instability threshold [9] of:

$$\Gamma_0^2 > \frac{V_{g_0} \gamma_0^2 k_A^2}{4 c_A} = \left[ \frac{1}{2} \sqrt{\frac{V_{g_0}}{c_A}} \gamma_0 k_A \right]^2, \tag{4.15}$$

When the group velocities are parallel, absolute growth is not possible. Convective growth may occur if $\Gamma_0^2 > (\gamma_0 k_A)(\gamma_{0_b} k_{0_b}) = 0$ since $\gamma_{0_b}$ is zero. The maximum growth rate [32] is then given by the solution to Eq. (4.12), for $\omega_{real} = k = 0$,

$$\Gamma_c = -\gamma_0 k_0 + \left[ \gamma_0^2 k_0^2 + \Gamma_0^2 \right]^{\frac{1}{2}} \simeq \Gamma_0. \tag{4.16}$$

This growth rate may be observed in an absolutely unstable plasma before the fastest modes have reached the boundaries. Convective instabilities correspond to limited amplification as compared to absolute instabilities. The absolutely unstable modes will grow until they are saturated by nonlinear effects or pump depletion. Equations (4.9) and (4.10) in the stationary approximation have the form

$$-i\mu_1 k_A \frac{\partial \bar{a}_{0_b}}{\partial x} = \mu_3 \bar{a}_0 \delta\bar{n}^*, \tag{4.17}$$

$$\gamma_0 k_A \delta\bar{n} + \frac{\partial \delta\bar{n}}{\partial x} = \frac{-i}{2} k_A \bar{a}_0 \bar{a}^*_{0_b}. \tag{4.18}$$

Assuming that $\frac{\partial \delta\bar{n}}{\partial x}$ is small, we solve Eqs. (4.17) and (4.18) for $\bar{a}_{0_b}$ to obtain:

$$\bar{a}_{0_b}(x) = \bar{a}_{0_b}(L) \exp\left(-\frac{\mu_3 \bar{a}_0^2}{2\mu_1 k_A \gamma_0}(x - L)\right). \tag{4.19}$$

where $\bar{a}_{0_b}(L)$ is the amplitude of the seed at the right side and $\gamma \cdot \delta\bar{n}$ has been replaced by $\gamma_0 k_A \delta\bar{n}$ from Eq. (1.7). Equation (4.19) leads to the definition of the gain, $G_0$, which is $a_{0_b}$ at $x = 0$. The gain is defined as:

$$G_0 = \frac{\mu_3 |\bar{a}_0|^2 L}{2\mu_1 k_A \gamma_0} = \frac{v_{osc}^2 n_{0_e}}{4 v_{th}^2 n_c} \frac{k_0 L}{\gamma_0 (1 - \frac{n_{0_e}}{n_c})}, \tag{4.20}$$

where $|\bar{a}_0|^2 = |\bar{a}_0(x = 0)|^2 = v_{osc}^2 / 4 v_{th}^2 = 0.5 P_0$. The gain is the exponent in the amplification factor for the seed. For an inhomogeneous plasma the gain [34] takes the following form:

$$G_g = \frac{\mu_3 |\bar{a}_0|^2 L}{2\mu_1 k_A h} = \pi \frac{v_{osc}^2 n_{0_e}}{4 v_{th}^2 n_c} \frac{k_0 L}{h (1 - \frac{n_{0_e}}{n_c})}. \tag{4.21}$$

Notice that the homogeneous gain coefficient depends inversely on damping while the inhomogeneous gain coefficient depends inversely on the gradient instead.

When the group velocities are anti-parallel, the second square root term in Eq. (4.14), produces another $+i$ since a $-i$ would create damping, this results in a

maximum absolute growth rate for the undamped system of:

$$\Gamma_{abs_0} = \Gamma_0 \frac{2\sqrt{V_{g_0} c_A}}{V_{g_0} + c_A} \cong 2\Gamma_0 \sqrt{\frac{c_A}{V_{g_0}}}. \tag{4.22}$$

A more exact expression is found in [33], where the analysis includes the spatial derivatives while damping and the finite system length are taken into account. The growth rate now becomes:

$$\Gamma_{abs} = \left( \frac{2\Gamma_0}{\sqrt{V_{g_0}}} \left( 1 - \frac{1}{\sqrt{\pi}\lambda^{\frac{2}{3}}} \right) - \frac{\gamma_0 k_A}{c_A} \right) \frac{V_{g_0}}{V_{g_0} + c_A} \tag{4.23}$$

where $\lambda = G_g/\pi$ should be greater than one.

## 4.2 Three Wave Model of SBS in Inhomogeneous Plasmas

The present model, Eqs. (4.1) and (4.2), must reproduce the previous results, in particular the solution by Rosenbluth [34], to the linearized three wave interaction in an inhomogeneous plasma. An analytic solution to the linearized set of Eqs. (4.1) and (4.2) was obtained by Rosenbluth in Refs. [34] and [35]. He has shown that a gradient would limit the size of the interaction region, by disturbing the matching conditions, Eqs. (1.15) and (1.16), to produce a finite gain coefficient, even though the plasma was arbitrarily large. A simplification suggested by V. Tikhonchuk where the propagation of sound waves is neglected, will be used here to recover Rosenbluth's solution. This reduces the resulting equation for the backscattered electrostatic field to a first order differential equation and the inverse Laplace transform of the solution, allows us to solve for the reflectivity at the left boundary. Dropping the nonlinear term in the KdV equation results in the equations:

$$i\frac{\partial a}{\partial t} + \mu_1 \frac{\partial^2 a}{\partial^2 x} + \mu_2 a = \mu_3 a \delta n \tag{4.24}$$

$$\frac{\partial \delta n}{\partial t} + \gamma_0 k_A \delta n + \left( 1 + \frac{h}{L}(x - x_0) \right) \frac{\partial \delta n}{\partial x} + \frac{1}{2}\frac{\partial^3 \delta n}{\partial x^3} = -\frac{1}{2}\frac{\partial |a|^2}{\partial x}. \tag{4.25}$$

We simplify Eqs. (4.24) and (4.25) by using Eqs. (4.5) and (4.6) and the matching conditions, Eqs. (1.15) and (1.16). With the above definitions and after gathering terms with like powers, Eqs. (4.24) and (4.25) become:

$$i\frac{\partial \bar{a}_{0_b}}{\partial t} - i\mu_1 k_A \frac{\partial \bar{a}_{0_b}}{\partial x} = \mu_3 \bar{a}_0 \delta\bar{n}^* \tag{4.26}$$

$$\frac{\partial \delta\bar{n}}{\partial t} + \gamma_0 k_A \delta\bar{n} + \left( ik_A \left( \frac{h}{L}(x - x_0) - \frac{k_A^2}{2} \right) \right) \delta\bar{n} + \frac{\partial \delta\bar{n}}{\partial x} = -\frac{i}{2} k_A \bar{a}_0 \bar{a}^*_{0_b}. \tag{4.27}$$

Dropping the spatial derivative in Eq. (4.27), and applying the Laplace transform, $F(x,p) = \int_0^\infty \exp(-pt)F(t,x)dt$, we may solve for $\delta\bar{n}^*_p$

$$\delta\bar{n}^*_p = \frac{\frac{i}{2}k_A \bar{a}^*_0 \bar{a}_p}{p + \gamma_0 k_A - ik_A \left( \frac{h}{L}(x - x_0) - \frac{k_A^2}{2} \right)}. \tag{4.28}$$

Applying the transform to Eq. (4.26) results in:

$$ipa_p - i\mu_1 k_A \frac{\partial \bar{a}_p}{\partial x} = \mu_3 \bar{a}_0 \delta\bar{n}_p. \tag{4.29}$$

Combining Eq. (4.28) and (4.29) yields a first order differential equation for $\bar{a}_p$:

$$\frac{\partial \bar{a}_p}{\partial x} - \frac{1}{\mu_1 k_A} \left( p - \frac{\frac{k_A}{2}\mu_3 |\bar{a}_0|^2}{p + \gamma_0 k_A - ik_A \left( \frac{h}{L}(x - x_0) - \frac{k_A^2}{2} \right)} \right) \bar{a}_p = 0. \tag{4.30}$$

Solving Eq. (4.30) for $\bar{a}_p(x,p)$ results in:

$$\bar{a}_p(0,p) = \bar{a}_p(L,p) \exp\left( -\frac{pL}{\mu_1 k_A} \right) \left[ \frac{p + \gamma_0 k_A - ik_A \left( \frac{h}{L}(L - x_0) - \frac{k_A^2}{2} \right)}{p + \gamma_0 k_A + ik_A \left( \frac{hx_0}{L} + \frac{k_A^2}{2} \right)} \right]^{iG_g/\pi}, \tag{4.31}$$

where $\bar{a}_p(L,p)$ represents the value of the seed at the right hand boundary, $G_g$ is defined in Eq. (4.21), and $P_0/2 = |\bar{a}_0|^2$ is the electric field intensity at the left boundary. Applying the inverse Laplace transform, $F(x,t) = (1/2\pi i)\int_C \exp(pt)F(x,p)dp$,

results in

$$\bar{a}_{0_b}(0) = \int_C dp \frac{\exp(pt)}{p + i\omega_{seed}} \exp\left(-\frac{pL}{\mu_1 k_A}\right) \left[\frac{p + \gamma_0 k_A - ik_A\left(\frac{h}{L}(L - x_0) - \frac{k_A^2}{2}\right)}{p + \gamma_0 k_A + ik_A\left(\frac{hx_0}{L} + \frac{k_A^2}{2}\right)}\right]^{iG_g/\pi} \tag{4.32}$$

where $\bar{a}_p(L,p)$ has been replaced by $(p + i\omega_{seed})^{-1}$, and $\omega_{seed} = k_A$ which corresponds to the ion acoustic frequency, $\omega = k_A(1 + V(x))$, at the point where the flow vanishes. Transforming to a dimensionless integration variable, $p = ik_A h/2\,(1 - \tilde{p}) - ik_A\,(hx_0/L + k_A^2/2)$, results in:

$$\bar{a}_{0_b}(0) = \exp\left[\frac{i2\tilde{t}}{h}\left(\frac{h}{2} - \left(\frac{hx_0}{L} + \frac{k_A^2}{2}\right)\right)\right] \frac{1}{2\pi i} \int_C d\tilde{p} \frac{\exp\left(i\tilde{p}\tilde{t}\right)}{\tilde{p} + \Omega} \left[\frac{\tilde{p} + i\tilde{\gamma} + 1}{\tilde{p} + i\tilde{\gamma} - 1}\right]^{iG_g/\pi} \tag{4.33}$$

where $\Omega$=$(1 - 2/hk_A\,(hx_0/L + k_A^2/2) + 2\omega_{seed}/hk_A)$, $\tilde{t}$=$k_A h/2\,(t - L/\mu_1 k_A)$, and $\tilde{\gamma}$= $2\gamma_0/h$. The solution to Eq. (4.33) requires that all of the poles be included in the contour integral, which is not too difficult since $\tilde{\gamma}$ is always less than one. The reflectivity is equal to $R(t) = |\,\bar{a}_{0_b}(x = 0)\,|^2/|\,\bar{a}_0(x = 0)\,|^2$. Figure 4.1 shows a comparison between the reflectivity from the KdV solution and that predicted by Eq. (4.33). The agreement in Fig. 4.1 shows that the reflectivity has the expected linear behavior.

## 4.3 Results of Numerical Simulations

The evolution of SBS in an inhomogeneous plasma is dependent on the combination of the gradient and damping strengths. We will first discuss SBS in a homogeneous plasma [24] followed by the weakly damped inhomogeneous plasma.

The dynamics of SBS reflectivity, in the case of strong damping and a homogeneous plasma, which is shown in Fig. 4.2, is given by the solution to the linearized, stationary Eq. (4.19), since we are below absolute threshold, Eq. (4.15). The net

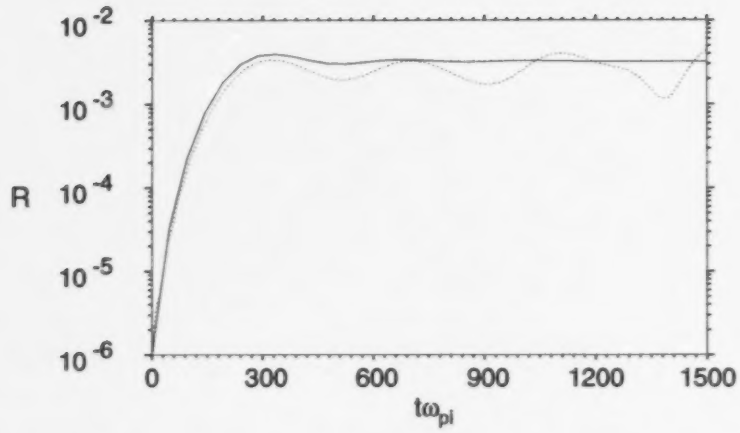


Figure 4.1: *Comparison between the reflectivity observed from the KdV equation, (dotted line), and the reflectivity predicted by by Eq. (4.33), (solid line). The parameters chosen are* $h = 0.2$, $\gamma_0 = 0.0117$, *and* $P_0 = 0.03$.

$e$-folding is given by

$$R = \frac{\mid \bar{a}_{0_b}(x=0,t=0) \mid^2}{\mid \bar{a}_0(x=0,t=0) \mid^2} \exp(2G_0) = R_0 \exp(2G_0)\,, \tag{4.34}$$

where $G_0$ is defined in Eqs. (4.20) for a homogeneous plasma and $R_0 = 10^{-6}$ . The exponent in Eq. (4.34) should be $> 1$. The reflectivity predicted by Eq. (4.34) is $1.1 \times 10^{-3}$, which compares with the observed value from the numerical simulation of $0.94 \times 10^{-3}$.

The SBS reflectivity from a homogeneous plasma, for weakly damped sound waves ($\gamma_0 = 0.0117$) is shown in Fig. 4.3. The modulations of reflectivity at the early times are related to the nonlinear evolution of sound waves. They grow to relatively high amplitudes, Fig 4.4, become nonlinear and change in time propagating from the left boundary to the right. Until these periodic soliton-like structures, which originate at $x = 0$ reach the right boundary , (i.e. for $t \lesssim 4000/\omega_{p_i}$), and establish stationary density profiles Fig. 4.4, the reflectivity displays transient time variations.

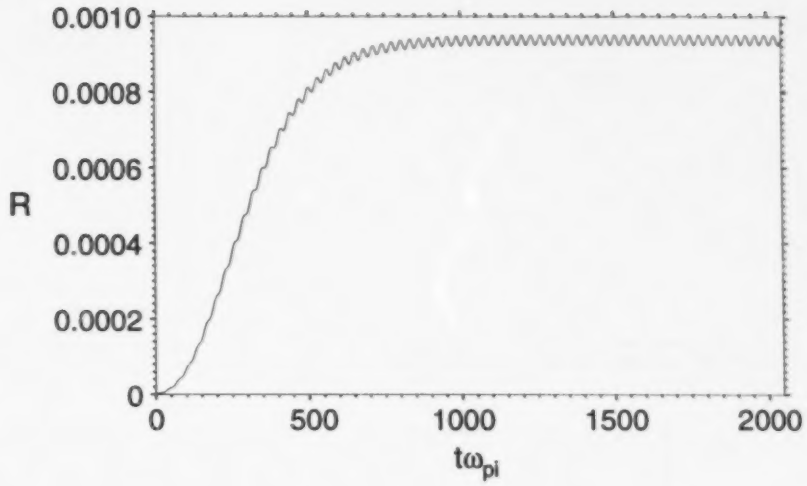


Figure 4.2: *The reflectivity in the case of strong damping, for the parameters:* $h = 0$, $\gamma_0 = 0.08$, *and* $P_0 = 0.03$.

The spatial modulations of the density perturbations, Fig. 4.4, at small values of $x$ have resulted from this dynamical evolution of nonlinear sound waves.

Figure 4.4 shows the large amplitude, nonlinear sound waves propagating to the right at the late time ($t = 8196/\omega_{p_i}$), corresponding to the stationary plateau on the reflectivity plot, Fig. 4.3. The density profile is also stationary. Its Fourier transform is shown in Fig. 4.5. The dominant sound wave at $k = 0.21k_D$ corresponds to the resonant mode satisfying the SBS matching conditions Eqs. (1.15) and (1.16). Higher order harmonics in Fig. 4.5 are the result of the nonlinear behavior of sound waves. The biggest amplitude ion acoustic perturbations occur at the left boundary, Fig. 4.4, where the electromagnetic wave amplitudes are also reaching their maximum, Fig. 4.6. The stationary plateau of the reflectivity for $t > 4000/\omega_{p_i}$ cannot be approximated by Eq. (4.19) due to the dominance of pump depletion and nonlinear effects.

The behavior of SBS for weakly damped ion waves and an inhomogeneous

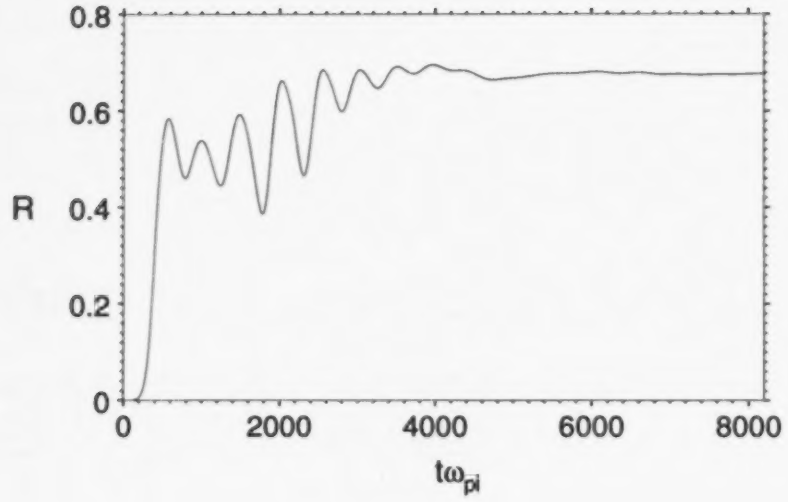


Figure 4.3: *The reflectivity, for the parameters:* $h = 0$, $\gamma_0 = 0.0117$, *and* $P_0 = 0.03$.

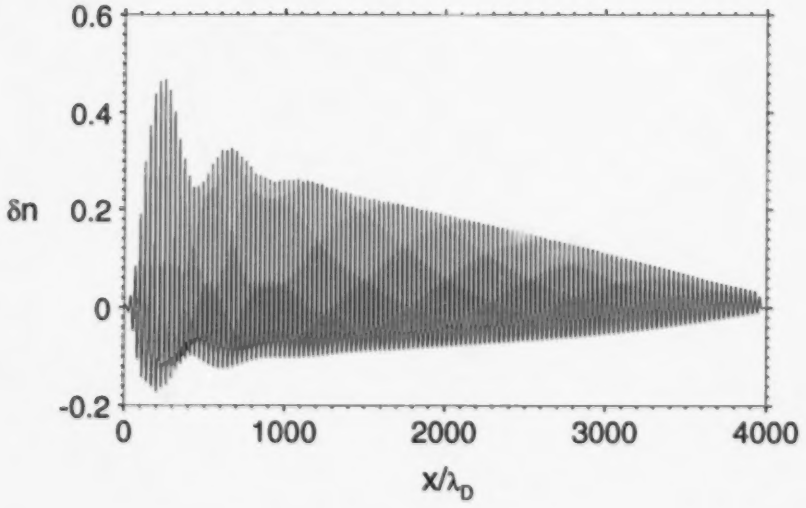


Figure 4.4: *Density at* $T = 8196$, *for the parameters shown in Fig. 4.3.*

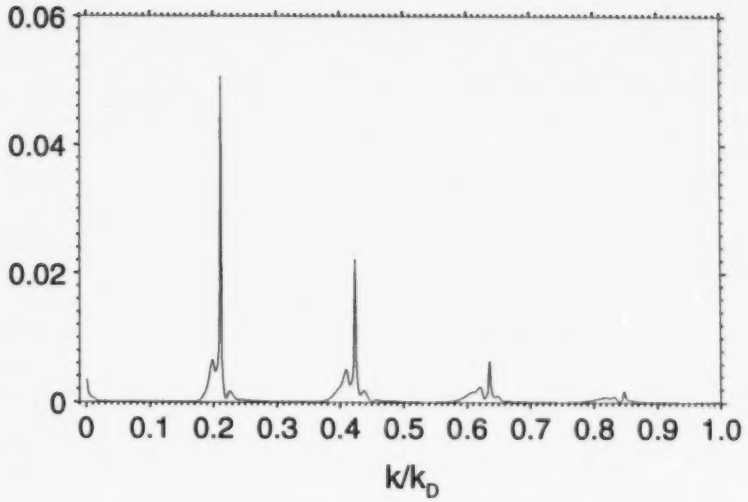


Figure 4.5: *Fourier transform of the density, for the parameters shown in Fig. 4.3.*

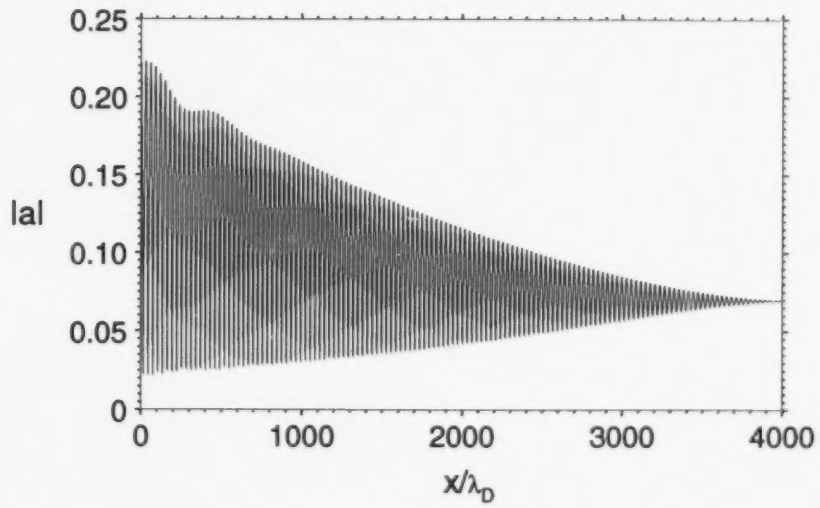


Figure 4.6: *Electric field amplitude at* $T = 8196$*, for the parameters shown in Fig. 4.3.*

plasma displays many different features as compared to the homogeneous case. Figure 4.7 combines results from the homogeneous (dashed line) and inhomogeneous (dotted line) runs. It also shows comparison with theoretical results obtained from the three wave coupling model in inhomogeneous plasmas, Eq. (4.33) ( dot-dashed line), and analytical theory of absolute instability in the finite inhomogeneous plasma (solid line), Eq. (4.23) [33]. At first reflectivity shows identical exponential growth in time for both the homogeneous and inhomogeneous plasma. At the relatively low reflectivity levels, defined approximately by the inhomogeneous gain, Eq. (4.21), the reflectivity experiences saturation due to the effect of the inhomogeneous flow velocity. The level is in partial agreement with the Rosenbluth theory, Ch. 4.2. However this analytical result, Eq. (4.21) is only valid in plasmas with no boundaries, which is certainly different from our numerical model based on finite simulation box. Indeed, approximately at the time when the first sound waves created at the left side of the plasma reach the right boundary the SBS starts to grow again with absolute growth rate, (dotted line), found in Ref. [33]. The growth rate described by Eq. (4.23) follows closely the numerical results in Fig. 4.7. It is an absolute growth, taking place at every point in the plasma, as one can see from the electric field profile in Fig. 4.8 and the density profile in Fig. 4.9, taken at $t = 3000/\omega_{p_i}$. After this period of temporal growth the reflectivity reaches a quasistationary state for $t \geq 4000/\omega_{p_i}$, at an average level of about 40% as one can see from Fig. 4.10. By comparing the plasma results in Fig. 4.10 one can see the important role of the inhomogeneous flow velocity.

The long time behavior of the SBS reflectivity, Fig. 4.10, in an inhomogeneous plasma displays an almost periodic oscillations. They can be related to the interesting evolution of the density perturbations and ponderomotive potential, shown in Figs. 4.8-4.16, at three different moments in time, corresponding to the first broad period in SBS reflectivity, Fig. 4.10, for $4000 < t\omega_{p_i} < 7000$. At the begining, ($t \cong 4000/\omega_{p_i}$), the main growth of scattered light occurs at the left boundary, Fig. 4.11, within

the region allowed by the velocity gradient, Fig. 4.12. The sound waves reach there relatively high amplitudes, and start to propagate to the right. The small rate of damping allows the characteristic triangle like structure of the density perturbations to propagate the length of the plasma with almost no change in amplitude. However, when the perturbations leave their original resonance region, they do not satisfy the SBS matching conditions with the same electromagnetic scattered wave. This results in the minima of reflectivity, which occur with a period corresponding to the ion wave crossing time.

An important feature of the reflected light is related to the frequency shift and the spectral width as seen at the left boundary. This charateristic is often used by experimentalists to indentify scattering instabilities in plasmas [6]. Figures 4.17 and 4.18 show the frequency spectra of the backscattered light from a homogeneous, Fig. 4.3, and inhomogeneous plasma Fig. 4.10, respectively. The spectrum shown in Fig. 4.17 illustrates typical properties of the homogeneous plasma interaction, i.e. narrow frequency spread and shift with respect to the pump frequency corresponding to a single ion acoustic resonance wave. The addition of an inhomogeneous flow velocity term allows all frequencies between $+h\omega_A/2$ and $-h\omega_A/2$ to grow as seen in Fig. 4.18.

Figure 4.19 shows a summary of reflectivity from the KdV electromagnetic wave equations, Eqs. (4.1) and (4.2), from several runs for different velocity gradients, $h$. Each value of the gradient has two symbols because the top row of symbols corresponds to average value of the reflectivity for large times, while the bottom row is the average value of the reflectivity from Eqs. (4.1) and (4.2), corresponding to the intermediate saturation predicted by the Rosenbluth theory. The deviation from the solid line, Eq. (4.34), is due to the break down of the linear theory. The evolution of SBS is not affected when multiple seed waves with random phases are introduced.

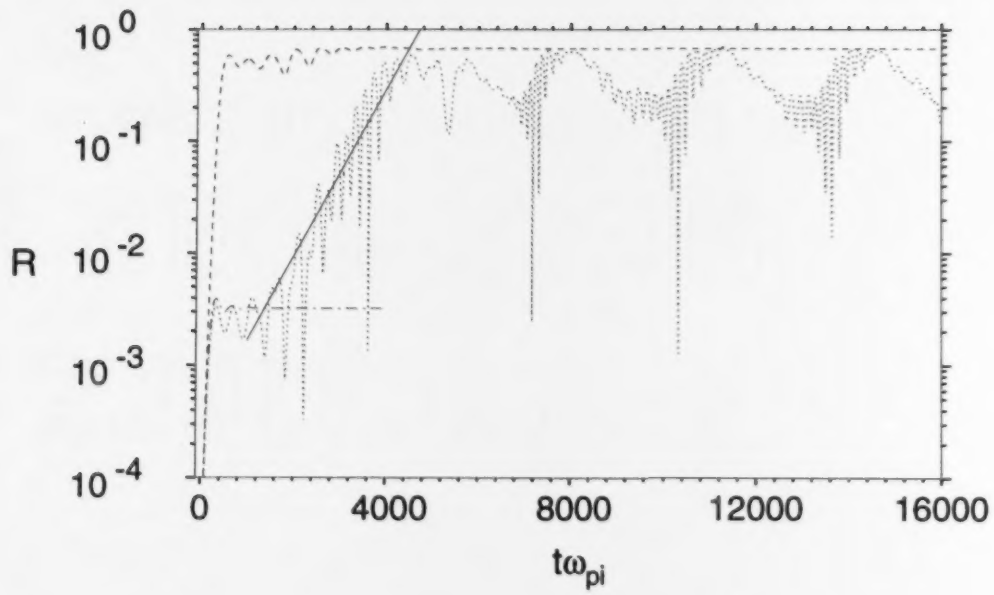


Figure 4.7: *Comparison between reflectivities obtained from the homogeneous and inhomogeneous plasmas. The dashed line is for conditions given in Fig. 4.3 for* $h = 0$, *the dotted line corresponds to* $h = 0.2$, *while the dot dashed line is Eq. (4.33) and the solid is Eq. (4.23). Notice that the gradient has lowered the average reflectivity, but it is not that dramatic. A more detailed picture of the early time development was shown in Fig. 4.1.*

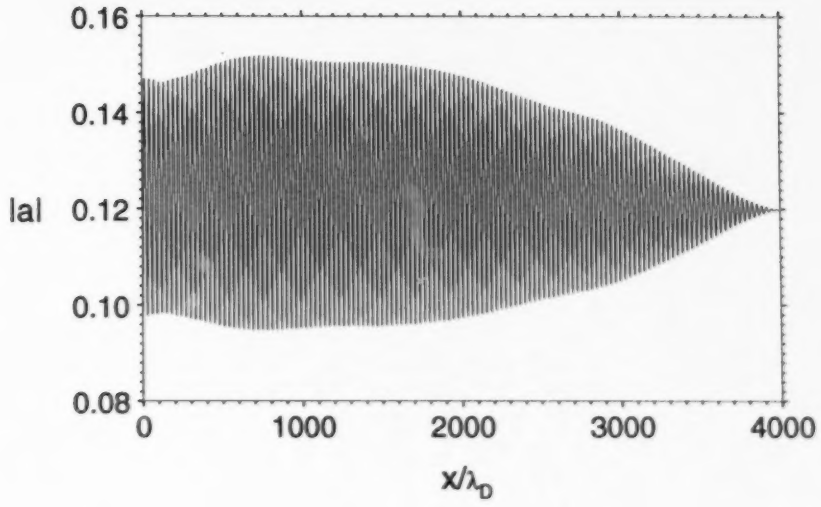


Figure 4.8: *The electric field at $T = 3000$, at the mid point of absolute growth. The parameters chosen are $h = 0.2$, $\gamma_0 = 0.0117$, and $P_0 = 0.03$.*

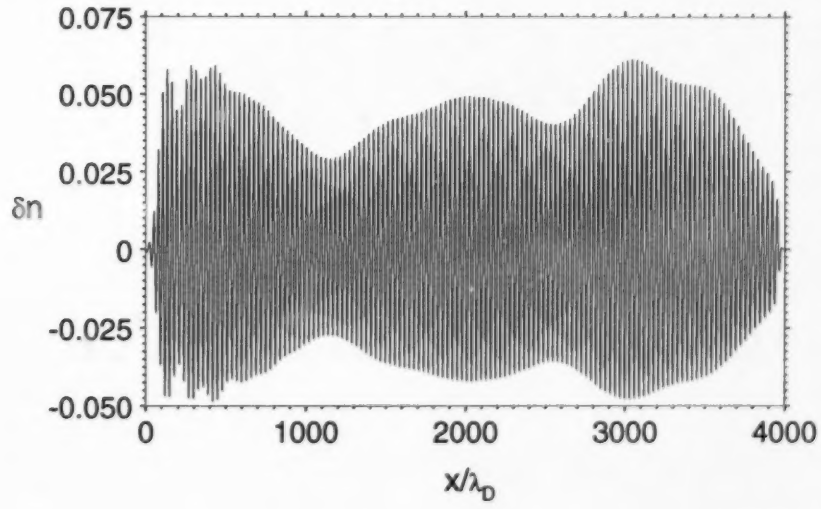


Figure 4.9: *Density at $T = 3000$, at the mid point of absolute growth, for the parameters shown in Fig. 4.8.*

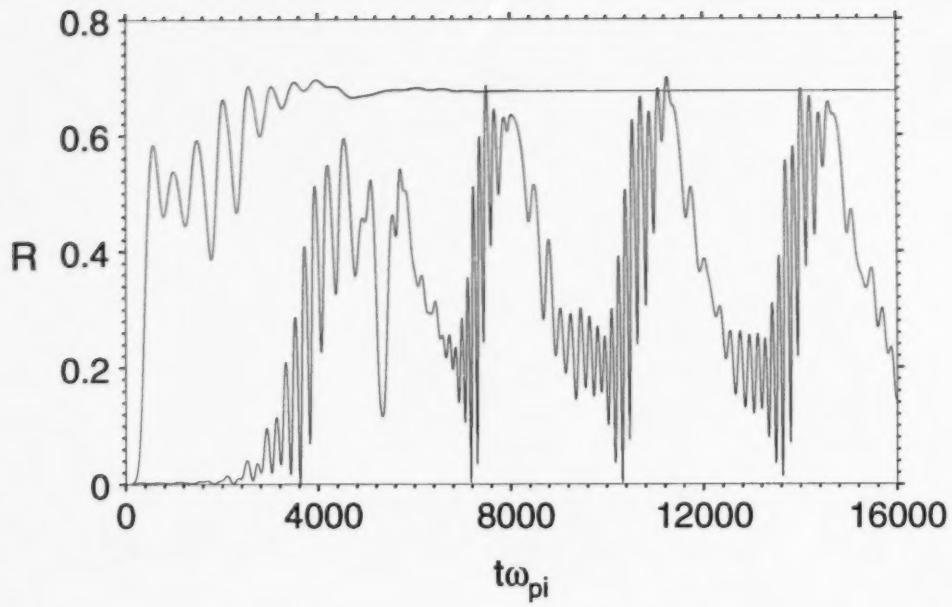


Figure 4.10: *Comparison between the homogeneous and inhomogeneous reflectivities for long times of Fig. 4.7. The upper line is for the conditions in Fig 4.3, while the lower line was Fig. 4.7, (dotted line).*

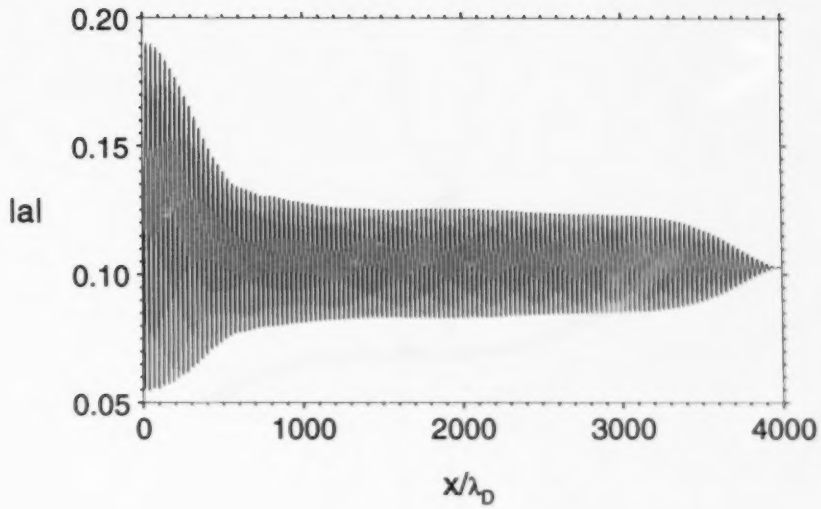


Figure 4.11: *Electric Field at* $T = 4096$, *for the parameters shown in Fig. 4.8.*

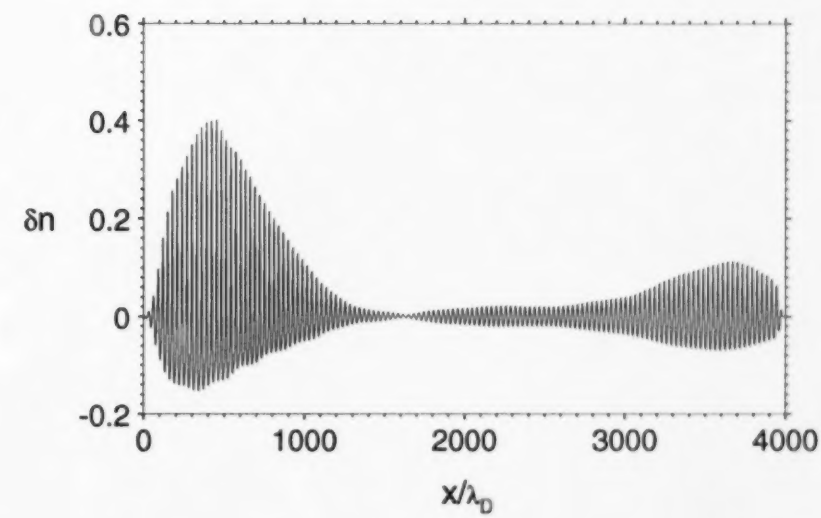


Figure 4.12: *Density at* $T = 4096$, *for the parameters shown in Fig. 4.8.*

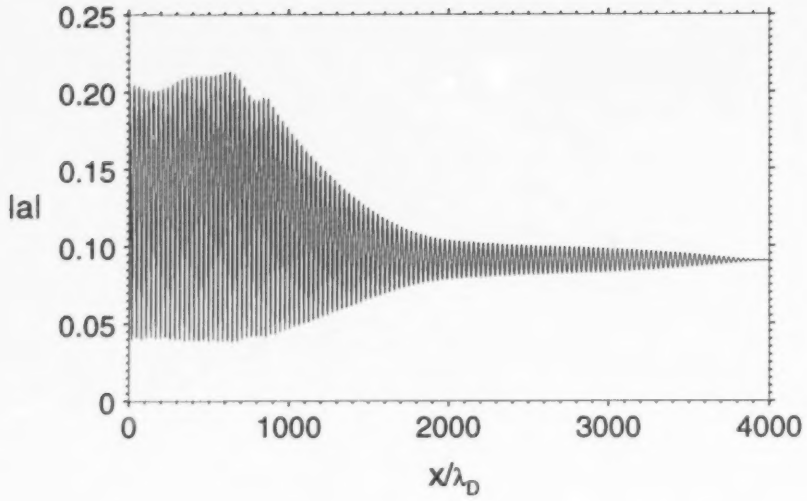


Figure 4.13: *Electric Field at $T = 5000$, for the parameters shown in Fig. 4.8.*

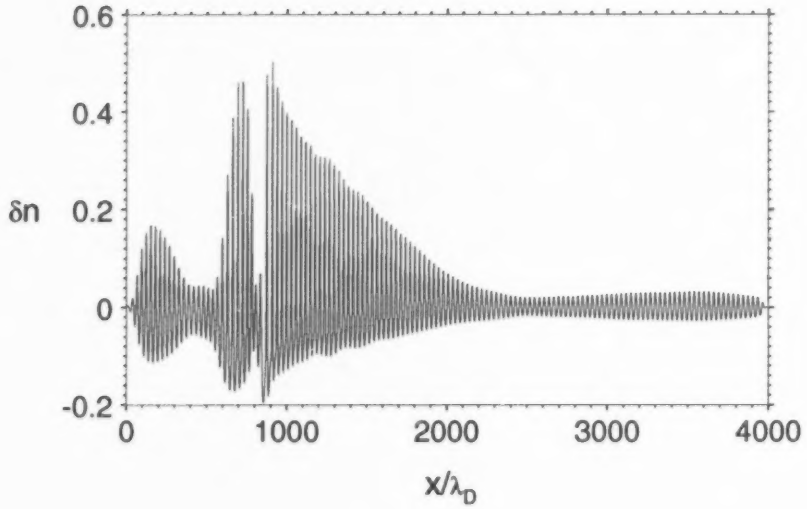


Figure 4.14: *Density at $T = 5000$, for the parameters shown in Fig. 4.8.*

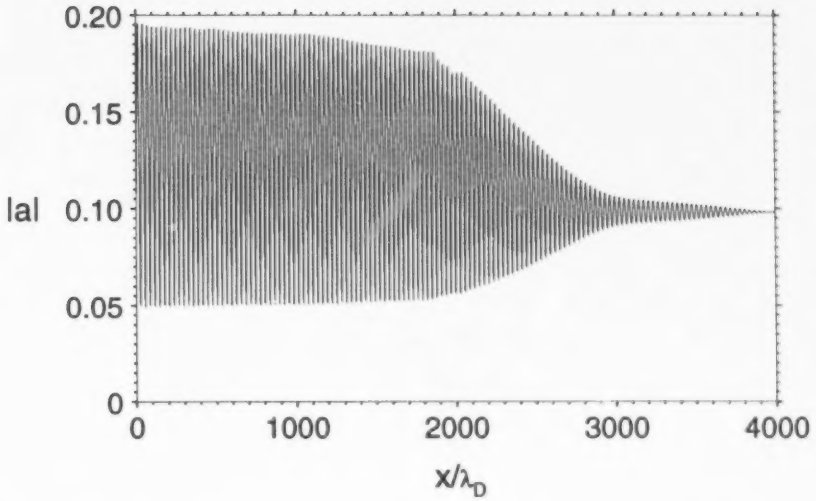


Figure 4.15: *Electric Field at* $T = 6144$, *for the parameters shown in Fig. 4.8.*

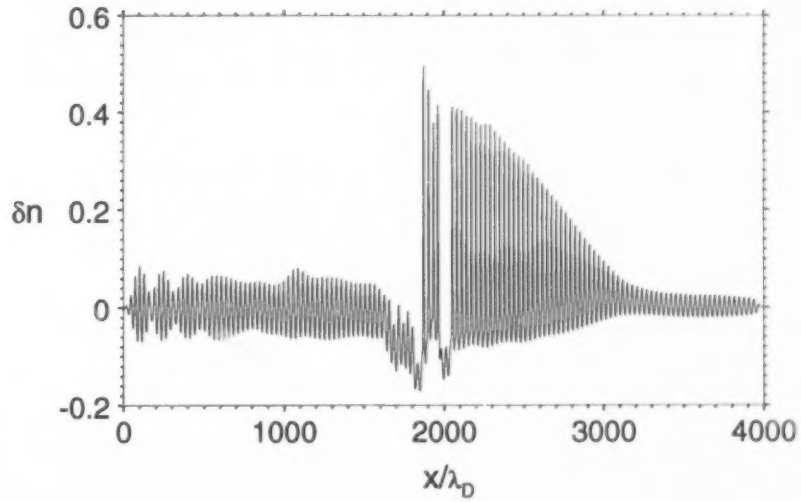


Figure 4.16: *Density at* $T = 6144$, *for the parameters shown in Fig. 4.8.*

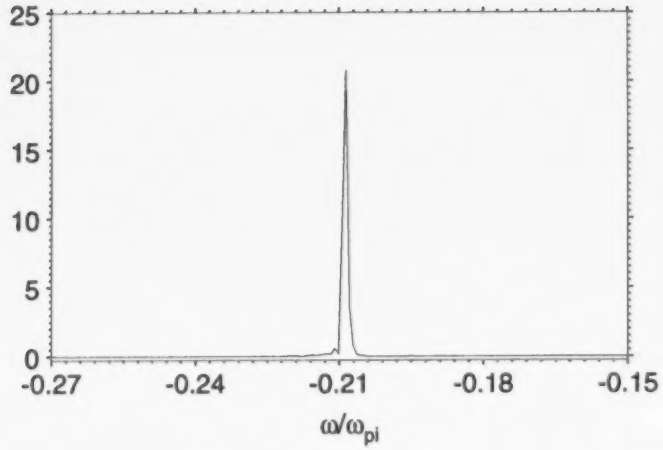


Figure 4.17: *Frequency spectrum of the reflected light from a homogeneous plasma, for the reflectivity shown in Fig. 4.3.*

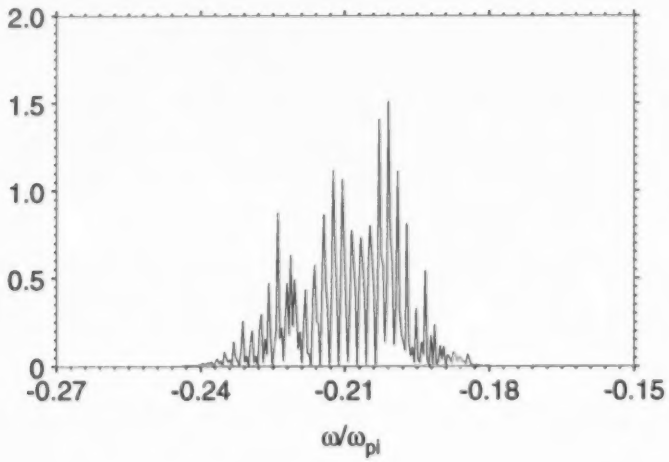


Figure 4.18: *Frequency spectrum of the reflected light from an inhomogeneous plasma, for the reflectivity shown in Fig. 4.7, (dotted line). The broadening of the frequency spectrum is due to the continuum of resonance points, the apparent discreetness is due to the finite resolution.*

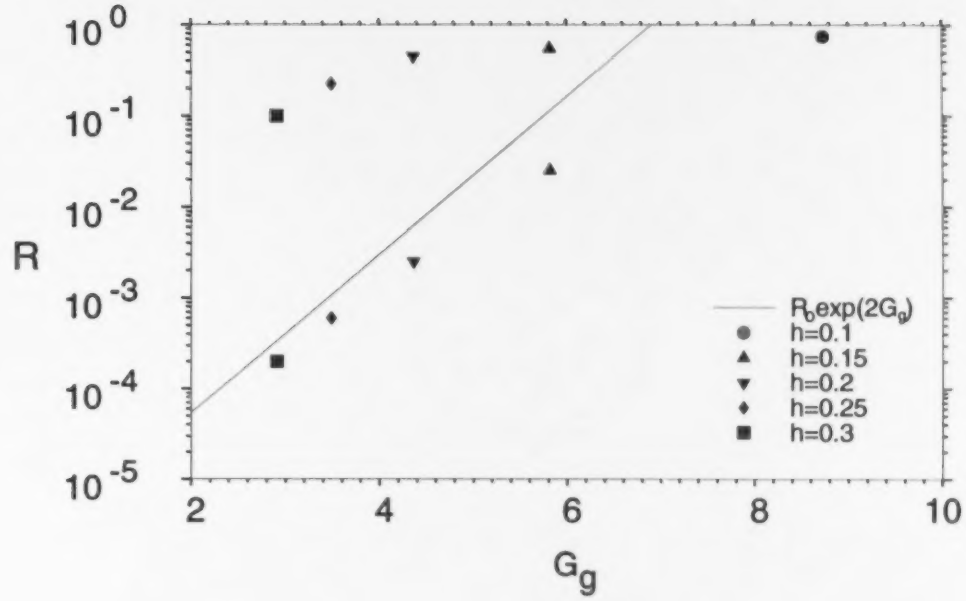


Figure 4.19: *Comparison of reflectivity from the KdV electromagnetic wave equations, Eqs. (4.1) and (4.2), for various values of h at selected times. The top row of repeated symbols corresponds to average value of the reflectivity for large times, while the bottom row is the average value of the reflectivity taken at the saturation of the Rosenbluth stage, which is defined by Eq. (4.33).*

# CHAPTER FIVE

# SUMMARY AND CONCLUSION

A stimulated scattering instability in an expanding laser plasma has been studied. The investigation has considered the influence of nonlinear sound waves and an inhomogeneous flow velocity on stimulated Brillouin scattering (SBS) in the regime of weakly damped ion acoustic waves. The theoretical model consists of an electromagnetic wave equation with a nonlinear coupling term and the Korteweg-de Vries equation (KdV), with an inhomogeneous velocity added to the sound speed. Numerical simulations and analytical calculations have been carried out in both the local approximation, Eq. (3.1), and for the full system of coupled equations, (4.1) and (4.2).

The local approximation, in which we have examined the KdV equation with a periodic driver of a constant amplitude, has been used to investigate the autoresonance process. As formulated by Friedland and Kaufman autoresonance occurs due to the cancellation between the nonlinear frequency shift of ion acoustic waves and the frequency shift produced by the inhomogeneous flow. The autoresonance effect, as predicted by [23], has been observed in the two harmonic approximation Eqs. (3.6) and (3.7), and shown in Figs. 3.11. It has not emerged, however, from the KdV solution, Fig. 3.12. Even in the two harmonic approximation, autoresonance has not been found in a region that is considered physically relevant. The minimum sound wave damping rate predicted by Eq. (1.7) is $\gamma_L = \sqrt{\pi Z m_e/8m_i}k$=0.01$k$, while to fulfill the autoresonance conditions, Eq. (3.23), it was necessary to reduce the damping rate to 0.003$k$. For a small value of the inhomogeneous flow parameter, $\mid h/L \mid$, the equivalence between a velocity and a density gradient was shown.

We have demonstrated for the first time that the combined effects of an in-

homogeneous flow velocity and of nonlinear behavior of sound waves can reduce SBS reflectivity. We have recovered the theoretical results obtained before [28], for the linear evolution of SBS. For homogeneous or nearly homogeneous plasmas, saturation can occur due to pump depletion and nonlinear effects or strong damping.

Evolution of stimulated Brillouin scattering depends on the ion wave damping. In homogeneous plasmas two different behaviors of SBS has been observed corresponding to convective or absolute instability. For a strong enough damping rate so that the pump intensity is below absolute threshold, Eq. (4.15), reflectivity is described by the convective gain, Eq. (4.16) and shown in Fig. 4.2. For weak damping and the pump above absolute threshold, Eq. (4.15), SBS reflectivity grows in time to high levels, until the instability is saturated by pump depletion and nonlinearity of sound waves as shown in Fig. 4.3. Characteristic time oscillations in the reflectivity curve, Fig. 4.3, correspond to nonlinear evolution of sound waves, which vary in time as they propagate through the plasma. The stationary solution is reached after the ion acoustic wave transient time, $t = L/c_A$.

The evolution of SBS in the presence of a moderate flow gradient produces different features as compared to the homogeneous case. At first the reflectivity shows identical exponential growth in time for both the homogeneous and inhomogeneous plasma, Fig. 4.7. At early times the reflectivity experiences saturation due to the effect of the inhomogeneous flow velocity, given by Eq. (4.21). As the sound waves propagate from the resonance point, a stage of absolute growth may occur, given by Eq. (4.23), if allowed by damping. The long time behavior of the SBS reflectivity is nonstationary and dominated by the dynamics of the nonlinear density perturbations. A combination of nonlinear, pump depletion, and flow gradient effects has saturated SBS . The SBS reflectivity oscillates with a period which is comparable to the the travel time of sound waves across the plasma. These oscillations are produced by a characteristic triangle like structure of the density perturbations which propagate the

length of the plasma with almost no change in amplitude due to small damping rate, Figs. 4.8 to 4.16. A summary of the results is shown in Fig. 4.19. It demonstrates that an increase in the inhomogeneous flow decreases the average SBS reflectivity.

The flow gradient also broadens the frequency spectrum of the reflected light, Fig. 4.18, as compared with the homogeneous case, Fig. 4.17. The frequency broadening is due to the existence of a continuum of resonance points in the inhomogeneous plasmas. At each point, which is characterized by a different value of a flow velocity, SBS excites ion acoustic waves of $k_A \simeq 2k_0$ with slightly different frequencies $\omega_A \simeq 2k_0 c_A(x)$. A difference between $\omega_A$ at the left and right plasma boundaries defines the width of a scattered light frequency spectrum observed in the simulation.

The velocity gradient in the coupled KdV-electromagnetic wave equations improves the theoretical predictions of reflectivity, but the theory is not complete enough to bring it in line with experimental observations.

# BIBLIOGRAPHY


[1] R. C. Davidson, *Methods in Nonlinear Plasma Theory*, Academic Press, New York, (1972).

[2] S. Ichimaru, *Statistical Plasma Physics Volume 1: Basic Principles*, Addison-Wesley, Don Mills, (1992).

[3] F. F. Chen, *Introduction to Plasma Physics and Controlled Fusion Vol. 1*, Plenum Press, New York., (1984).

[4] E. Infeld and G. Rowlands, *Nonlinear Waves, Solitons and Chaos*, Cambridge University Press, Cambridge, (1990).

[5] W. L. Kruer, *The Physics of Laser Plasma Interactions*, Addison-Wesley, New York, (1988).

[6] H. A. Baldis, E. M. Campbell, and W. L Kruer, in *Handbook of Plasma Physics*, edited by A. Rubenchik and S. Witkowski (North-Holland, Amsterdam), **3** 361 (1991).

[7] C. S. Lui, K. Nishikawa, in *Advances in Plasma Physics*, Edited by A. Simon and W. B. Thompson, John Wiley & Sons, New York, (1976).

[8] R. P. Drake, Lasers and Particle Beams, **10**, 599 (1992).

[9] K. Mima, K. Nishikawa, in *Handbook of Plasma Physics*, Edited by A. A. Galeev and R. N. Sudan, North Holland, New York, **2**, 451 (1984).

[10] Ph. Mounaix, D. Pesme, W. Rozmus, and M. Casanova, Phys. Fluids B**5**, 3304 (1993).

[11] W. L. Kruer, Phys. Fluids **23**, 1273 (1980).

[12] D. W. Forslund, J. M. Kindel, and E. L. Lindman, Phys. Fluids **18**, 1002 (1975).

[13] D. W. Forslund, J. M. Kindel, and E. L. Lindman, Phys. Fluids **18**, 1017 (1975).

[14] R. L. Berger, Phys. Fluids **27**, 1796 (1984).

[15] S. S. Shen, *A course on Nonlinear Waves*, Kluwer Academic Publishers, Dordrecht, (1993).

[16] M. R. Amin, C. E. Capjack, P. Frycz, W. Rozmus, V. T. Tikhonchuk, Phys. Fluids B**5**, 3748 (1993).

[17] V. V. Eliseev, W. Rozmus, V. T. Tikhonchuk, and C. E. Capjack, *Stimulated Brillouin Scattering and Ponderomotive Self-Focusing from a Single Laser Hot Spot*, Phys. of Plasmas **2**, in press (1995).

[18] D. J. Korteweg and G. de Vries, Phil. Mag. **39**, 422 (1895).

[19] E. Fermi, J. Pasta and S. Ulam, "Studies in Nonlinear Problems," Los Almos Scientific Laboratory Report, LA (1940).

[20] N. J. Zabusky and M. D. Kruskal, Phys. Rev. Lett. **15**, 240 (1965).

[21] H. A. Baldis, D. M. Villeneuve, B. LaFontaine, G. D. Enright, C. Labaune, S. Baton, Ph. Mounaix, D. Pesme, M. Casanova, and W. Rozmus, Phys. Fluids B**5**, 3319 (1993).

[22] L. Friedland, Phys. Rev. Lett. **69**, 1749 (1992).

[23] L. Friedland, A. N. Kaufman, *Autoresonant Stimulated Brillouin Scattering*, preprint (1992).

[24] W. Rozmus, M. Casanova, D. Pesme, A. Heron, and J.-C. Adam, Phys. Fluids B**4**, 576 (1992).

[25] V. P. Silin and V. T. Tikhonchuk, Sov. Phys. JEPT Lett. **34**, 365 (1981).

[26] J. A. Heikkinen, S. J. Karttunen, and R. R. E. Salomaa, Phys. Lett. **101A**, 217 (1984).

[27] J. A. Heikkinen, S. J. Karttunen, and R. R. E. Salomaa, Phys. Fluids, **27**, 207 (1984).

[28] J. Candy, W. Rozmus, and V. T. Tikhonchuk, Phys. Rev. Lett. **65**, 1889 (1990).

[29] V. V. Kurin, Sov. J. Plasma Phys. **8**, 207 (1982).

[30] M. Casanova, G. Laval, R. Pellat, and D. Pesme, Phys. Rev. Lett. **54**, 2230 (1985).

[31] A. Bers, in *Handbook of Plasma Physics*, Edited by A. A. Galeev and R. N. Sudan, North Holland, New York, **1**, 451 (1983).

[32] D. E. Hinkel, E. A. Williams and R. L. Berger, Phys. Plasmas **1**, 2987 (1994).

[33] D. F. DuBois, D. W. Forslund, and E. A. Williams, Phys. Rev. Lett. **33**, 1013 (1974).

[34] M. N. Rosenbluth, Phys. Rev. Lett. **29**, 565 (1972).

[35] M. N. Rosenbluth, R. B. White, and C. S. Liu, Phys. Rev. Lett. **31**, 1190 (1973).

[36] T. Kolber, PhD thesis *Scattering Instabilities in Laser Plasmas*, University of Alberta, Edmonton, Appendix .3 (1993).

# APPENDIX A

# NUMERICAL CONSIDERATIONS

The numerical solution to Eqs. (4.1) and (4.2) requires that we make certain assumptions and approximations. The boundary conditions chosen are:

$$\frac{\partial \delta n}{\partial t} = \frac{\partial \delta n}{\partial x} - \eta(x)\delta n,$$

$$0 = i\frac{\partial a}{\partial x} + k_0\left(2a_0 - a\right) \tag{A.1}$$

at the left boundary, $x = 0$, and

$$\frac{\partial \delta n}{\partial t} = \frac{\partial \delta n}{\partial x} - \eta(x)\delta n,$$

$$0 = i\frac{\partial a}{\partial x} - k_0 a - k_A a_s \exp\left(i\left(2k_0\left[1 - 2k_0^2\right]t + \phi_0\right)\right) \tag{A.2}$$

at the right boundary, $x = L$, where $\eta(x)$ is defined in Eq. (A.3) and $\phi_0$ is a small constant phase. A seeded left going wave, $a_s$, with an amplitude $10^{-3}a_0$, is introduced at the right boundary.

A five point finite difference scheme is used to discretise Eqs. (4.1) and (4.2) in the center of the box , while a four point difference scheme is used for the boundaries, Eqs. (A.1) and (A.2). The five point finite differences are accurate to fourth order while the four point differences are accurate to second order. The nonlinear equations are integrated in time and iterated for every time step until the desired accuracy is achieved [36]. To prevent the reflected ion waves near the edges of the box some artifical damping was required. This damping coefficient takes the form as the sum of two Fermi functions:

$$\eta(x) = \eta_0\left(\frac{1}{1 + exp\left(\frac{x - x_L}{w_s}\right)} + \frac{1}{1 + exp\left(\frac{x_R - x}{w_s}\right)}\right) \tag{A.3}$$

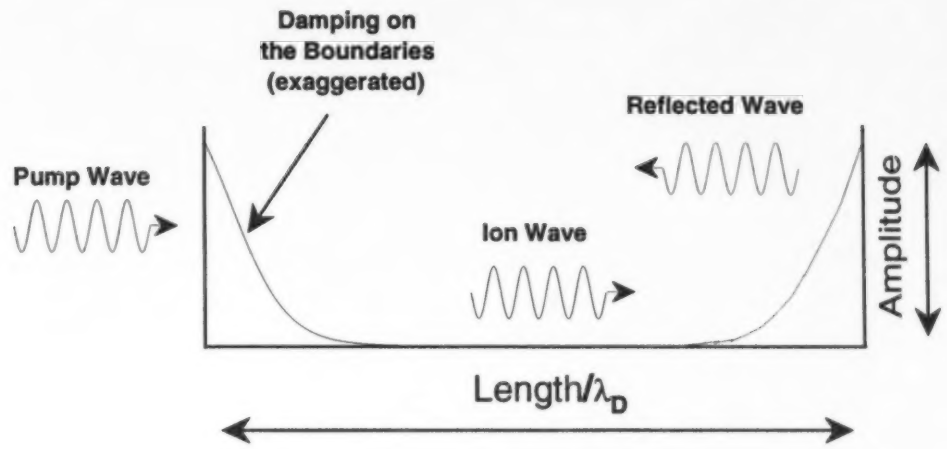


Figure A.1: *Schematic representation of the simulation box*

where $\eta_0$ is the maximum damping rate, $w_s$ is the steepness and $(x_L, x_R)$ are the center of the $(left, right)$, Fermi functions respectively. Landau damping is implemented in Fourier space by applying Eq. (1.7). The density is then obtained by using an inverse Fourier transform and inserting it back into the solver to begin the next time step. A schematic of the simulation box is shown in Fig. A.1.

Typical parameters of our 1-D plasma are: $n_{0_e}/n_c$=0.15, $Z$=10, $T_e$=1keV, $T_i$=0.5keV, and $x_0 = 2000$. These physical parameters determin a wave vector of $k_A = 0.21$ and predict a Landau damping rate of $0.0117 \times k_A = \gamma_0 k_A$. If we choose $\lambda_0$=1.0$\mu$m then $L = 4000\lambda_D = 67\lambda_0$, $I = 1.5 \times 10^{14} \frac{W}{cm^2}$, $\frac{1000}{\omega_{p_i}}$=72ps, and the inhomogeneous flow, $h = 0.2$, is 20% across the plasma. A. Baldis, C. Labaune, et. al. at Ecole Polytechnique and O. Willi et. al. at Rutherford Lab, predict a value for the SBS reflectivity, $R$, at a few percent.

# APPENDIX B

# THE EQUIVALENCE OF THE DENSITY AND VELOCITY GRADIENTS IN THE LOCAL APPROXIMATION

We have found that the results of Ch. 3 can be reproduced if we replace the velocity gradient by a density gradient. We know that the density inhomogenities are felt directly by the electromagnetic wave, through the electron plasma frequency (1.5). We will show that they can also directly affect SBS produced ion acoustic waves.

Density inhomogenities are responsible for the $x'$ dependance of $k_0(x')$ and $k_{0_b}(x')$, Eq. (1.5), which results in the $k_0(x') - k_{0_b}(x')$ being approximated by $k_A(1 + \int^{x'} D(y)dy)$, where $D(x')$ represents the density variation in $x'$. The KdV equation then takes the following form:

$$\frac{\partial \delta n}{\partial t'} + \gamma_L \delta n + \frac{\partial \delta n}{\partial x'} + \frac{\partial (\delta n)^2}{\partial x'} + \frac{1}{2}\frac{\partial^3 \delta n}{\partial x'^3} = P\, Im\left\{\exp\left(i(k_A x' - \omega_A t' + \int^{x'} D(y)dy + \phi_0)\right)\right\}, \tag{B.1}$$

where $\gamma_L$ is Landau damping, Eq. (1.7), $P$ is the constant amplitude driver, $\phi_0$ an arbitrary constant phase, and $\delta n$ is the real density perturbation. If we assume that $D(x') = hk_A(x' - x_0)/L$ is a linear function of $x'$, Eqs. (3.1) and (B.1) can be related through the following transformation:

$$x = x' + \frac{h}{2L}(x' - x_0)^2; \qquad t = t'. \tag{B.2}$$

The partial derivatives then transform as follows:

$$\frac{\partial}{\partial t'} = \frac{\partial}{\partial t}; \qquad \frac{\partial}{\partial x'} = (1 + \frac{2h}{L}(x - x_0))^{\frac{1}{2}} \frac{\partial}{\partial x} \tag{B.3}$$

where we have only taken the positive root in Eq. (B.3). Substituding Eq. (B.3) into Eq. (B.1) yields the following expression:

$$\frac{\partial \delta n}{\partial t} + \gamma_L \delta n + (1 + \frac{2h}{L}(x - x_0))^{\frac{1}{2}} \frac{\partial \delta n}{\partial x} + \frac{1}{2}(1 + \frac{2h}{L}(x - x_0))^{\frac{1}{2}} \frac{\partial (\delta n)^2}{\partial x} +$$

$$\frac{1}{2}(1 + \frac{2h}{L}(x - x_0))^{\frac{3}{2}} \frac{\partial^3 \delta n}{\partial x^3} = P \sin[k_A x - \omega t) + \phi_0], \tag{B.4}$$

where we have assumed that $\mid h/L \mid \ll 1$, which is always the case. Expanding the root in front of the convective term in Eq. (B.4) to linear order and taking only the zeroth order approximation by the other two terms because we do not want to involve higher order corrections, we get:

$$\frac{\partial \delta n}{\partial t} + \gamma_L \delta n + \left(1 + \frac{h k_A}{L}(x - x_0)\right) \frac{\partial \delta n}{\partial x} + \frac{\partial (\delta n)^2}{\partial x} + \frac{1}{2} \frac{\partial^3 \delta n}{\partial x^3} =$$

$$P \sin \{(k_A x - \omega_A t + \phi_0)\} \tag{B.5}$$

which is Eq. (3.1). A direct numerical comparison between the two cases showed that their was virtually no difference.